JCB Journal of Cell Biology

ARTICLE

Maize *defective kernel5* is a bacterial TamB homologue required for chloroplast envelope biogenesis

Junya Zhang[1], Shan Wu[2], Susan K. Boehlein[1,2], Donald R. McCarty[1,2], Gaoyuan Song[3], Justin W. Walley[3], Alan Myers[4], and A. Mark Settles[1,2]

Chloroplasts are of prokaryotic origin with a double-membrane envelope separating plastid metabolism from the cytosol. Envelope membrane proteins integrate chloroplasts with the cell, but envelope biogenesis mechanisms remain elusive. We show that maize *defective kernel5* (*dek5*) is critical for envelope biogenesis. Amyloplasts and chloroplasts are larger and reduced in number in *dek5* with multiple ultrastructural defects. The DEK5 protein is homologous to rice SSG4, *Arabidopsis thaliana* EMB2410/TIC236, and *Escherichia coli* tamB. TamB functions in bacterial outer membrane biogenesis. DEK5 is localized to the envelope with a topology analogous to TamB. Increased levels of soluble sugars in *dek5* developing endosperm and elevated osmotic pressure in mutant leaf cells suggest defective intracellular solute transport. Proteomics and antibody-based analyses show *dek5* reduces levels of Toc75 and chloroplast envelope transporters. Moreover, *dek5* chloroplasts reduce inorganic phosphate uptake with at least an 80% reduction relative to normal chloroplasts. These data suggest that DEK5 functions in plastid envelope biogenesis to enable transport of metabolites and proteins.

Introduction

Plastids are essential organelles for plants. Higher plants differentiate specialized plastids distinguished by structure, pigmentation, and function, such as photosynthetic chloroplasts in leaves and starch accumulating amyloplasts in the cereal endosperm (Jarvis and López-Juez, 2013). Plastids originated through endosymbiosis ∼1.5 billion years ago, when cyanobacteria were acquired by eukaryotic cells (Yoon et al., 2004). Extant cyanobacteria are Gram negative, with inner and outer plasma membranes. Chloroplasts also have a double-membrane structure, with inner and outer envelopes likely corresponding to bacterial membranes (Gould et al., 2008; Gross and Bhattacharya, 2009). The vast majority of chloroplast proteins are nuclear encoded, synthesized on cytosolic ribosomes, and imported into plastids post-translationally (Jarvis, 2008). These precursors are imported through the protein translocons of the outer and inner chloroplast envelope membranes, termed TOC and TIC, respectively (Keegstra and Cline, 1999; Cline and Dabney-Smith, 2008).

The plastid has a major role in primary metabolism (Bowsher and Tobin, 2001). Transport of solutes and metabolites across the envelope is important to integrate chloroplast metabolism with the cytosol and other cellular organelles. Chloroplast envelopes exchange ions, carbohydrates, nucleotides, and amino acids to support metabolic pathways in which the chloroplast has unique enzymatic activities (Block et al., 2007; Facchinelli and Weber, 2011).

The inner envelope has multiple solute translocators and is considered the primary metabolite permeability barrier (Flügge, 1999; Fischer, 2011). Inner envelope translocators are integral membrane proteins with two pathways for insertion. During protein import, some inner envelope membrane (IEM) proteins are transferred to the membrane through a stop-transfer mechanism. Other IEM proteins complete import into the stroma and are inserted similar to posttranslational translocation of secreted bacterial proteins (Li and Schnell, 2006; Tripp et al., 2007; Viana et al., 2010).

The outer envelope is thought to be permeable to solutes of <10 kD, which is similar to outer membranes of Gram-negative bacteria (Flügge and Benz, 1984). Porins facilitate this nonspecific diffusion of small solutes in Gram-negative bacteria (Nikaido, 1994). Many chloroplast outer envelope proteins (OEPs) have a β-barrel structure similar to porins and were

[1]Plant Molecular and Cellular Biology Program, University of Florida, Gainesville, FL; [2]Horticultural Sciences Department, University of Florida, Gainesville, FL; [3]Plant Pathology and Microbiology, Iowa State University, Ames, IA; [4]Roy J. Carver Department of Biochemistry, Biophysics, and Molecular Biology, Iowa State University, Ames, IA.

Correspondence to A. Mark Settles: settles@ufl.edu.

hypothesized to facilitate nonspecific diffusion; however, biochemical analyses show more selective transport. Pea OEP21 transports P_i, triose phosphates, and 3-phosphoglycerates (Hemmler et al., 2006). OEP24 allows diffusion of triose phosphates, dicarboxylic acids, charged amino acids, ATP, and P_i (Pohlmeyer et al., 1998). OEP40 is permeable to glucose, glucose-1-phosphate, and glucose-6-phosphate (Harsman et al., 2016). OEP16 and OEP37 are selective for amino acids and peptides and even have tissue specific expression patterns (Pohlmeyer et al., 1997; Goetze et al., 2006; Pudelski et al., 2012). Thus, OEP channels studied so far show specificity for distinct metabolites, challenging the notion that the outer envelope is a nonspecific molecular sieve.

Relatively little is known about the biogenesis pathways of β-barrel OEPs (Huang et al., 2011). In Gram-negative bacteria, most β-barrel outer membrane proteins require the β-barrel assembly machinery (β-BAM) for correct folding (Hagan et al., 2011; Selkrig et al., 2014). The translocation and assembly module (TAM) is also important for bacterial outer membrane biogenesis. TAM is composed of TamA, localized to the outer membrane, and TamB, localized to the inner membrane (Selkrig et al., 2012). Tam mutations in different bacterial species can alter membrane morphology or block secretion of toxins (Selkrig et al., 2012; Shen et al., 2014; Iqbal et al., 2016). Phylogenetic analysis showed that TamA is restricted to *Proteobacteria*, whereas TamB is widely distributed across Gram-negative bacteria (Heinz et al., 2015). In *Borrelia burgdorferi*, TamB interacts with a BAM subunit, suggesting that TamB participates in assembly of β-barrel proteins through multiple outer membrane protein assembly machineries (Iqbal et al., 2016).

Here, we show that the maize *defective kernel5* (*dek5*) mutant has plastid division defects that disrupt endosperm starch accumulation. Mutant *dek5* seedling leaves have fewer and larger chloroplasts with defects in chloroplast membranes. Molecular identification of the *dek5* locus demonstrated that it encodes a predicted TamB homologue. Contrary to a prior report for the rice DEK5 orthologue (Matsushima et al., 2014), the maize DEK5 protein is localized to the chloroplast envelope with analogous topology to TamB and the *Arabidopsis thaliana* DEK5 orthologue (Chen et al., 2018). The *dek5* mutant alters envelope ultrastructure, reduces OEP accumulation, alters inner envelope protein levels, and blocks P_i uptake. These data suggest that *Dek5* has a role in plastid envelope biogenesis and illustrate the importance of selective solute transport across the plastid envelope.

Results

Starch accumulation defects in *dek5* kernels

The Maize Genetics Cooperative Stock Center maintains six mutant alleles of the recessive *dek5* locus: *dek5-N874A*, *dek5-N961*, and *dek5-N1339A* isolated from ethyl methanesulfonate mutagenesis; *dek5-PS25* and *dek5-MS33* isolated from a *Robertson's Mutator* transposon-tagging population, and the spontaneous *dek5-Briggs* allele isolated at a commercial breeding company (Neuffer and Sheridan, 1980; Scanlon et al., 1994; Sachs, 2009). At maturity, each allele conditions shrunken or collapsed endosperm, while embryo development is frequently normal (Fig. 1 A). Among the alleles, *dek5-Briggs* and *dek5-N1339A* have more severe phenotypes. The visual phenotype of mature kernels resembles that of *brittle1* (*bt1*), *brittle2* (*bt2*), and *shrunken2* (*sh2*) mutants blocked in starch biosynthesis (Fig. 1 B). Unless noted, *dek5-MS33* was used for phenotype analysis.

Near-infrared reflectance spectroscopy analyses of mature kernels indicated *dek5* mutants have reduced starch and increased oil content compared with normal siblings (Fig. 1 C). The *dek5* starch deficiency is apparent in developing endosperm at 12 d after pollination (DAP) and extends to maturity (Fig. 1 D). Hand sections of developing kernels had uneven starch staining, even though mutants enlarged to a similar extent as normal siblings (Fig. 1 E). Like *bt1*, *bt2*, and *sh2*, the *dek5* endosperm collapses as mature kernels dry down. Relative zein content, particularly α-zein, is also reduced in *dek5* mutants (Fig. 1 F). Both *bt1* and *bt2* have reduced zein content associated with reduced starch (Lee and Tsai, 1984).

Soluble sugar levels are consistent with reduced accumulation of starch. At 20 and 24 DAP, *dek5* endosperm has elevated levels of sucrose, glucose, and maltose as well as higher levels of ADP-glucose at 24 DAP (Fig. 1 G). Sucrose, glucose, and ADP-glucose are soluble precursors of starch. On a fresh weight basis, sucrose and glucose are elevated similarly in *dek5*, *sh2*, and *bt1* with *dek5* sucrose and glucose being 4.2-fold and 3.4-fold higher than normal siblings, respectively (Tobias et al., 1992). The higher levels of ADP-glucose in *dek5* are similar to *sh2; bt1* double mutants (Shannon et al., 1996).

Endosperm starch granules have a normal diameter at 12 DAP but increase significantly in *dek5* at 24 DAP (Fig. 2, A and B). Mature endosperm granule size is 20% larger in *dek5* (Fig. 2 C). Reduced total starch concomitant with increased granule size implies *dek5* endosperm accumulates fewer granules than normal.

The average chain length distribution of the amylopectin component of endosperm starch was determined after enzymatically converting the branched polymer to a population of linear α(1→4)-linked glucan chains. The frequency of each length from 6 to 44 glucosyl units is essentially identical in *dek5* and normal siblings (Fig. 2 D). Despite enlarged granules, there is no apparent change in assembly of semicrystalline amylopectin.

Chloroplast defects in *dek5* plants

Depending upon the allele, 5–40% of *dek5* kernels germinate and seedlings have nonclonal, white variegation. Mutant seedlings are stunted at 7 d after sowing (DAS) and usually die in 2–3 wk (Fig. 3 A). Mo17 and W22 genetic backgrounds enhance *dek5*, resulting in a nearly empty pericarp kernel, lower germination, and more severe seedling phenotypes. The *dek5-Briggs* allele was the most severely modified (Fig. S1 A). By contrast, introgression of *dek5* into B73 improved grain-fill, germination, and mitigated seedling lethality (Fig. S1 B). The mild *dek5-MS33* allele could complete a life cycle to produce all mutant kernels (Fig. S1 C).

The pale green, variegated *dek5* leaves are due to multiple chloroplast abnormalities. Photosynthetic pigments and subunits of the electron transport chain are reduced (Fig. 3, B and C). Leaf protoplasts showed *dek5* mutants have larger and fewer

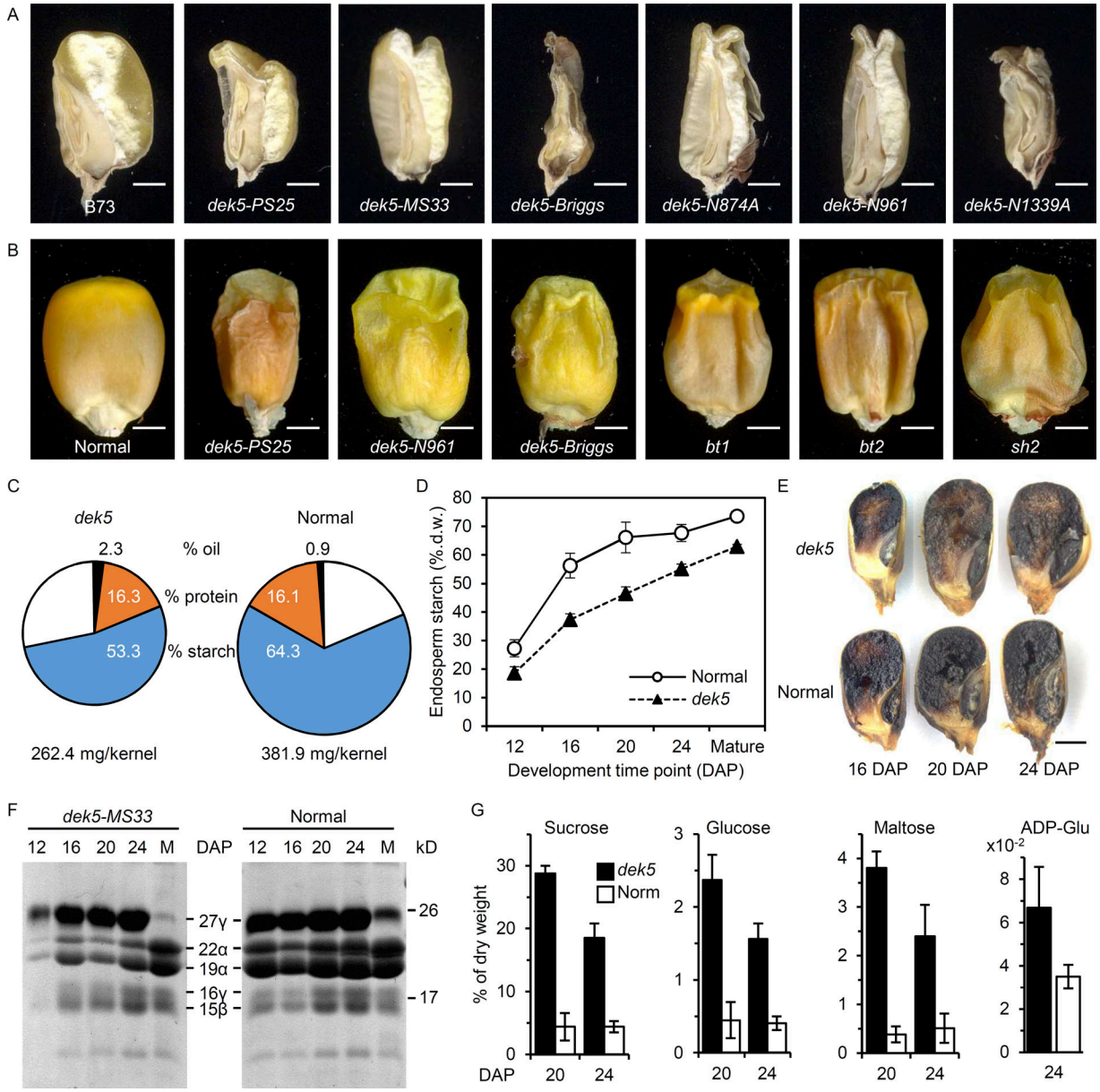

Figure 1. ***dek5* kernel phenotypes. (A)** Sagittal sections of mature kernels for normal (B73) and *dek5* alleles in B73. **(B)** Abgerminal view of mature kernels for normal, three alleles of *dek5*, and *bt1*, *bt2*, and *sh2* mutants. Scale bars are 2 mm. **(C)** Proportional pie charts of average mature composition and weight for 20 kernels of *dek5-MS33* and normal siblings. Percent oil is black; protein is orange; starch is blue; other constituents are white. **(D)** Mean and standard deviation of endosperm starch for *dek5* and normal siblings (n = 3 biological replicates). d.w., dry weight. **(E)** Iodine stained sagittal sections of developing kernels. Starch stains black. Scale bar is 2 mm. **(F)** Zein levels during development and at maturity (M). Protein was loaded on equal dry tissue weight. **(G)** Mean and standard deviation of endosperm metabolites (n = 3 biological replicates).

chloroplasts compared with normal siblings; a subset of mutant cells have one chloroplast or no chloroplasts (Fig. 3 D). Z-stack imaging of chlorophyll florescence showed *dek5* protoplasts have 7.5-fold fewer chloroplasts with a 6.6-fold increase in chloroplast volume (Fig. 3, E and F; and Video 1).

Mutant protoplasts isolated in standard buffers had a low recovery rate, while doubling mannitol to 0.8 M increased recovery nearly twofold (Fig. 3 G; Student's t test, P = 0.02). The *dek5* cells isolated in high osmotic buffer frequently contained multiple vacuolar compartments, which is a morphological characteristic of autophagy or programed cell death (Fig. 3 H; van Doorn et al., 2011). These data suggest that *dek5* cells are more likely to lyse with standard buffers and have altered osmotic pressure.

Transmission EM (TEM) revealed multiple ultrastructural defects in *dek5* chloroplasts. Chloroplasts in expanding maize seedling leaves develop in a gradient. At the base, differentiating plastids have few internal membranes, while chloroplasts at the middle and tip of the leaf have developed thylakoids (Pogson et al., 2015). Sections from the base, middle, and distal tip of *dek5* seedling leaves had much larger mesophyll chloroplasts with similar thylakoid development to normal siblings (Fig. 4,

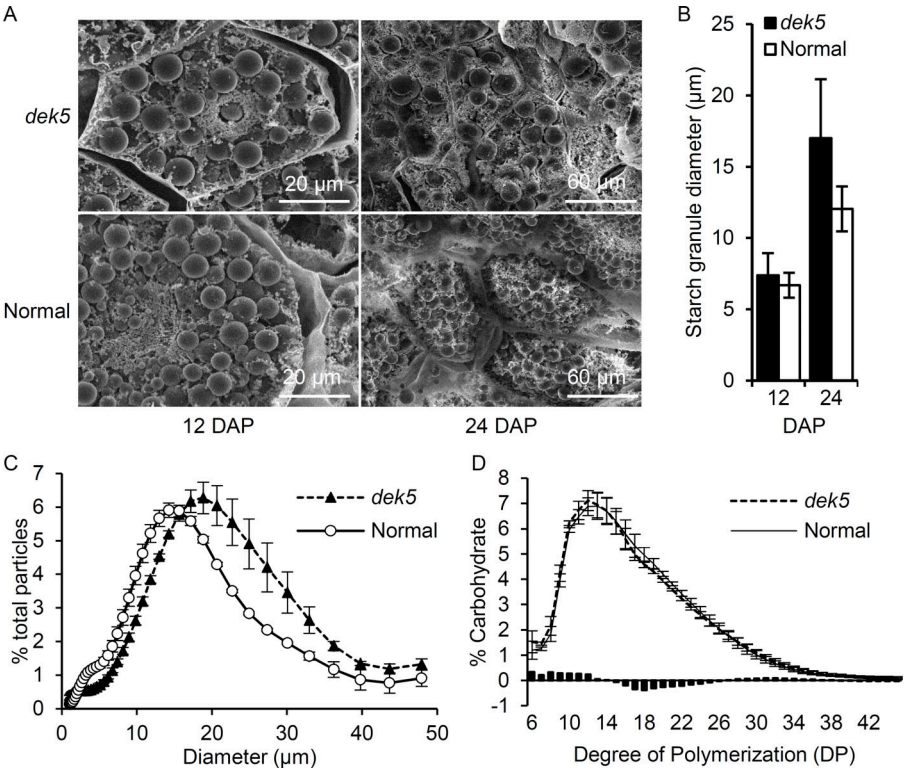

Figure 2. **Starch in *dek5* kernels. (A)** Scanning EM of starch granules in *dek5* and normal sibling endosperm. **(B)** Mean and standard deviation of starch granule diameter from three scanning EM images per condition (n = 38 [*dek5* 12 DAP], 77 [normal 12 DAP], 16 [*dek5* 24 DAP], and 11 [normal 24 DAP]). **(C)** Mean and standard deviation of mature endosperm starch granule size (n = 4 biological replicates). Particle sizes <1 µm and >50 µm are excluded. The plot accounts for 86% of total particles. **(D)** Mean and standard deviation of amylopectin chain-length distribution (n = 3 biological replicates). Bars plot the difference of normal minus mutant.

A–F). Normal chloroplasts have two thylakoid centers defining the long axis of the organelle (Fig. 4, B and C). In *dek5*, there are multiple thylakoid centers and a more spherical organelle shape (Fig. 4, E and F).

C4 plants, like maize, localize starch biosynthetic enzymes and starch granules in bundle sheath chloroplasts (Majeran et al., 2005; Leegood, 2008; Weise et al., 2011). Large starch granules were observed in normal bundle sheath chloroplasts at the tip of the leaf (Fig. 4 I). Mutant bundle sheath chloroplasts were much larger; however, these contained many vesicular structures with a few, small starch granules (Fig. 4 L). Some *dek5* mesophyll chloroplasts also had starch granules, which was not found in normal siblings (Fig. 4 F). These observations suggest defects in regulating starch synthesis or transporting fixed carbon to bundle sheath cells.

Consistent with protoplast imaging, *dek5* mesophyll chloroplasts have fourfold larger cross-sectional area than normal (Fig. 5 A). Although thylakoid grana appear normal, *dek5* grana are 40% larger in diameter, suggesting a higher proportion of the chloroplast develops as thylakoid (Fig. 5 B). Stromal area is threefold larger in *dek5* chloroplasts (Fig. 5 C). Comparing total and stromal area, the fraction of stroma in *dek5* is reduced by 20% relative to normal (Fig. 5 D).

The ratio of envelope to other chloroplast compartments is also altered in *dek5*. The cross-sectional area of the chloroplast could be modeled as an ellipse from long and short axis measurements (Fig. 5, E–H), suggesting that volume and surface area could be modeled as an ellipsoid. Estimates from TEM indicate a 14.7-fold increase in chloroplast volume and an 8.6-fold increase in stromal volume, but surface area only increases by 4.7-fold (Fig. 5, I–K). The surface area to volume ratios for *dek5* chloroplasts or stroma is reduced by threefold or twofold, respectively (Fig. 5, L and M). The increase in thylakoid with concomitant reductions in surface area suggests that *dek5* has a relative reduction in envelope membrane.

The more spherical shape and increased volume of *dek5* chloroplasts is not commonly reported in chloroplast division mutants. TEM analyses of division mutants show filamentous or buckled chloroplasts with a relatively normal short axis (Itoh et al., 2001; Ii and Webber, 2005; Karamoko et al., 2011; Kamau et al., 2015). Filamentous chloroplasts with a constant short axis can be roughly modeled as a cylinder, and surface area increases linearly with increased volume instead of the nonlinear relationship for ellipsoid-like *dek5* chloroplasts (Fig. 5 N). By contrast, the *A. thaliana tic40* mutant causes a more spherical chloroplast with a similar long axis to short axis ratio as *dek5* (Kovacheva et al., 2005). However, only the long axis of *tic40* chloroplasts is reduced, and *tic40* has predicted volume and surface area in the range of WT chloroplasts (Fig. 5 N). For ellipsoid-shaped organelles, the long/short axis ratio has relatively little impact on the surface area to volume ratio at a given volume (Fig. 5 O). Even though *dek5* and *tic40* have similar shapes, the low volume of *tic40* chloroplasts results in a typical surface area to volume ratio (Fig. 5 O). A chloroplast volume increase without forming filamentous or buckled organelles indicates a relative decrease in envelope.

TEM also revealed a range of membrane defects. Mutant chloroplasts had unusual envelope ingrowths as well as an expanded peripheral reticulum (Fig. 6, A–C; Szczepanik and Sowiński, 2014). Internal thylakoid membranes appeared disorganized in some chloroplasts (Fig. 6, D and E; and Fig. S2). In some cases, internal vesicles and completely disorganized plastids were

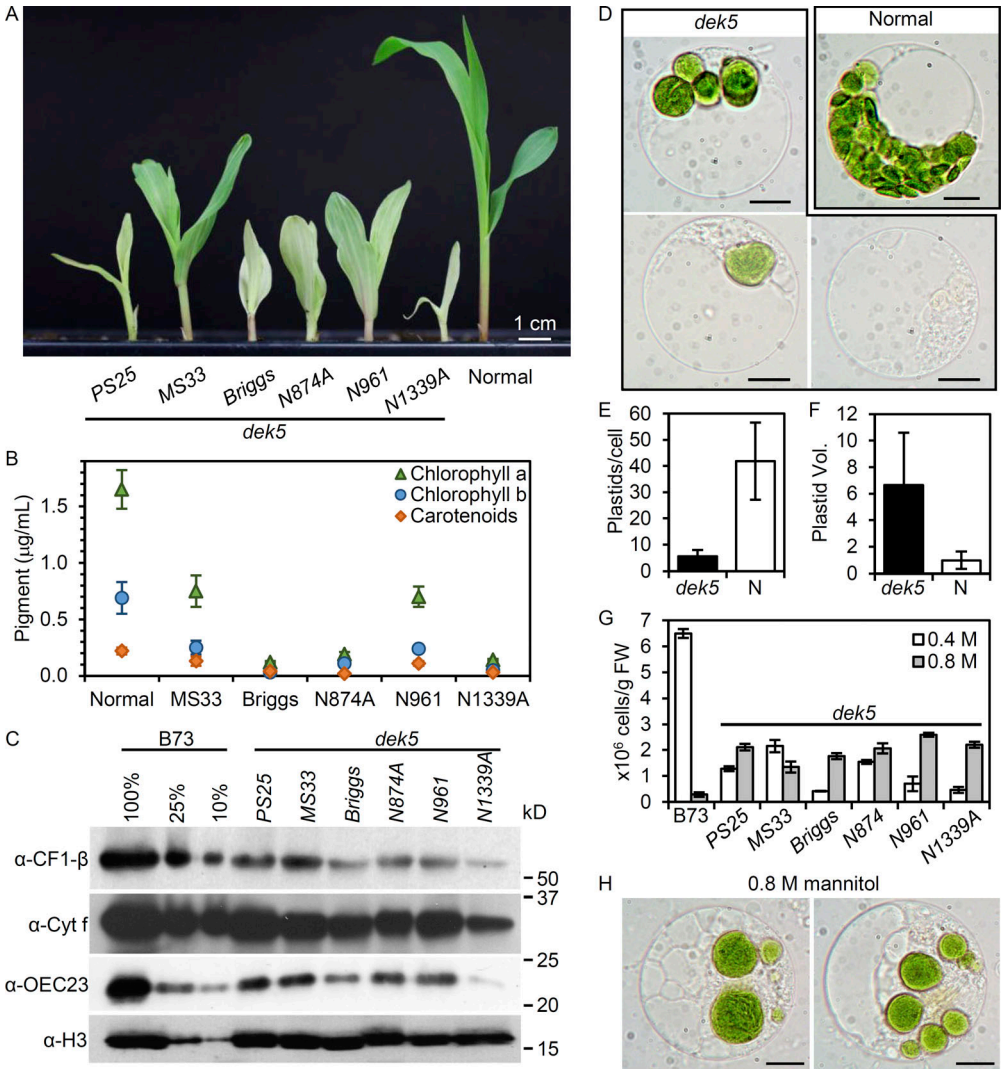

Figure 3. **Fewer and larger chloroplasts in *dek5* seedling leaf cells. (A)** Representative *dek5* seedlings. **(B)** Mean and standard deviation of seedling leaf photosynthetic pigments (n = 3 seedlings). **(C)** Immunoblots of photosynthetic subunits: Oxygen evolving complex 23-kD subunit (OEC23), Cyt f, and ATP synthase B (CF1-β). Histone 3 (H3) is a protein-loading control. Lanes have 5 µg of total leaf protein with dilutions for B73. **(D)** Mesophyll leaf protoplasts. Scale bars represent 10 µm. **(E)** Chloroplasts per protoplast from LCSM Z-stack imaging (n = 64 [*dek5*] and 60 [normal (N)] protoplasts). Error bars represent standard deviation. **(F)** Relative chloroplast volume from LCSM Z-stack imaging (n = 29 (*dek5*) and 29 (N) protoplasts). Error bars represent standard deviation. **(G)** Mean and standard error of protoplast yield with increased mannitol (n = 3 technical replicates). **(H)** *dek5* protoplasts isolated in 0.8 M mannitol. Scale bars are 10 µm.

observed (Fig. S2, E and F). The more severe phenotypes were observed immediately adjacent to cells with intact chloroplasts indicating that the defective membranes are unlikely to be an artifact from fixation or sample processing. Mutant chloroplasts with a loss of internal chlorophyll autofluorescence were also observed by laser confocal scanning microscopy in 16 of 51 *dek5* protoplasts that had full Z-stack imaging (Fig. 6, F–H; and Video 1). The data indicate that *dek5* has pleiotropic plastid membrane biogenesis defects.

Dek5 is homologous to *tamB*

The *dek5* locus was mapped to the short arm of chromosome 3 using B-A translocations (Neuffer and Sheridan, 1980). We fine-mapped the *dek5-PS25* allele to a genomic interval of 460 kbp containing 13 gene models in the B73 RefGen_v3 genome assembly (Fig. 7 A). Mu-Seq analysis of *Mutator* transposon insertions in *dek5-PS25* and *dek5-MS33* identified an insertion in GRMZM2G083374 (Fig. 7 B). There is a *Mu8*-like transposon in *dek5-PS25* and a *Mu1* insertion in *dek5-MS33* at the identical position in exon 1, indicating that these are independent alleles. The *dek5-Briggs* allele has a frameshift mutation with a single base insertion at exon 10 that results in a downstream premature termination codon. Two additional *Mu* insertion alleles from the UniformMu genetic resource failed to complement *dek5-PS25* (Fig. 7, C and D). Molecular identification of five noncomplementing alleles shows GRMZM2G083374 is the *dek5* locus.

The *dek5* genomic locus is predicted to be a single-copy gene that is >30 kbp. We amplified and sequenced the B73 cDNA to validate the predicted gene model. The sequenced *Dek5* mRNA

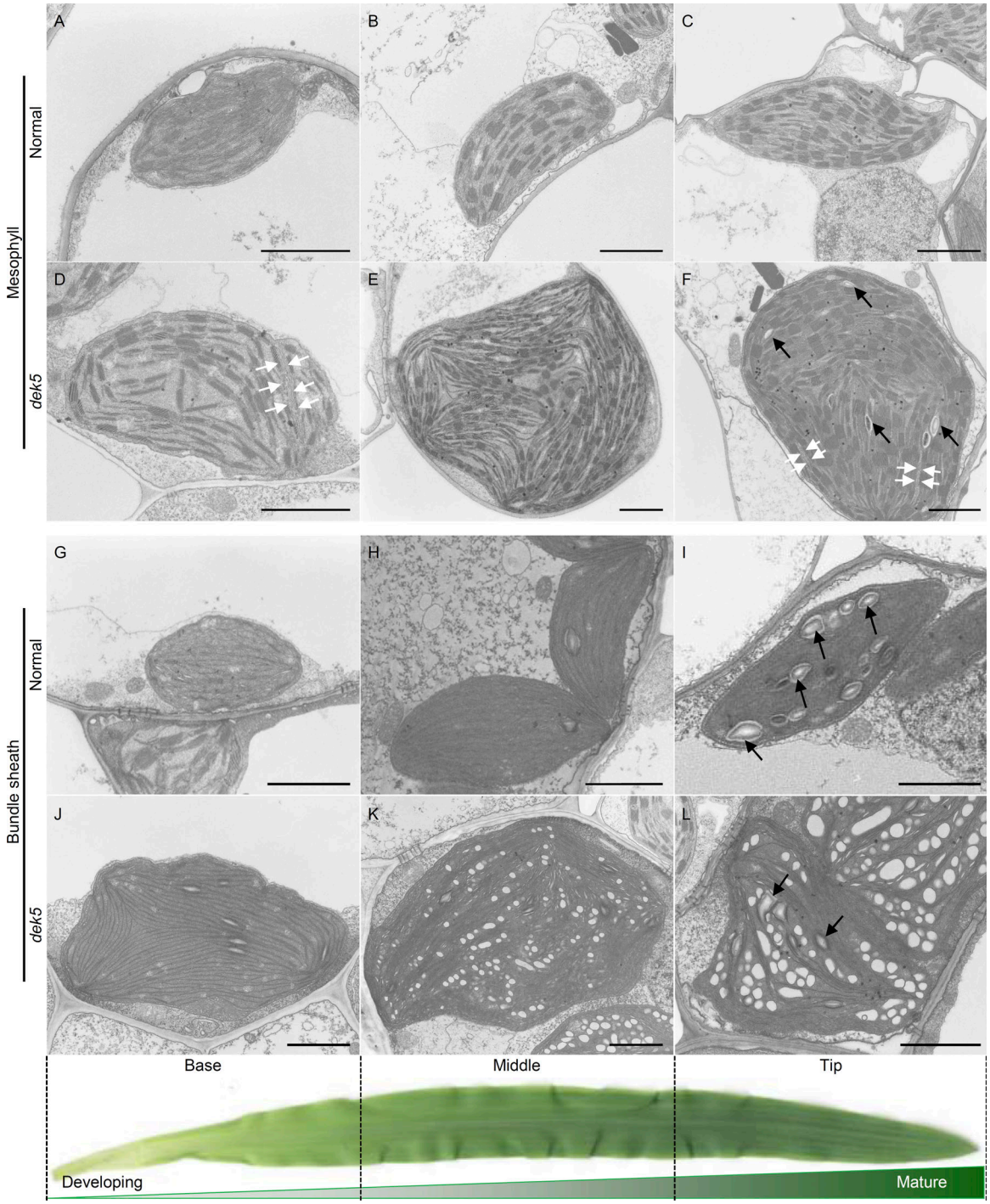

Figure 4. **TEM analysis of dek5 and normal sibling leaf chloroplasts. (A–C)** Normal mesophyll cell chloroplasts. **(D–F)** Mutant *dek5* mesophyll cell chloroplasts. White arrows indicate envelope ingrowths. Black arrows indicate starch granules. **(G–I)** Normal bundle sheath cell chloroplasts. **(J–L)** Mutant bundle sheath cell chloroplasts. In all panels, scale bars are 2 µm, and black arrows indicate starch granules.

has a different structure than GRMZM2G083374. It consists of 23 exons with a genomic transcriptional unit of 30,833 bp, which is identical to the current B73_v4 transcript model, Zm00001d039612_T001 (Fig. 7 B). *Dek5* encodes a predicted protein of 232.9 kD that has an N-terminal chloroplast transit peptide (TP), a transmembrane domain (TMD), and a C-terminal TamB domain, formerly DUF490 (Fig. 7 E). In rice, a missense mutation in the *Dek5* orthologue, *Substandard Starch Grain4* (*SSG4*), results in enlarged starch granules and chloroplasts similar to *dek5* (Matsushima et al., 2014). Loss of function of the *A. thaliana dek5* orthologue, *emb2410*, causes an embryonic lethal phenotype, while weak alleles (*tic236*) have been reported to reduce chloroplast protein import (Chen et al., 2018). The DEK5 domain structure is similar to the *Escherichia coli* TamB

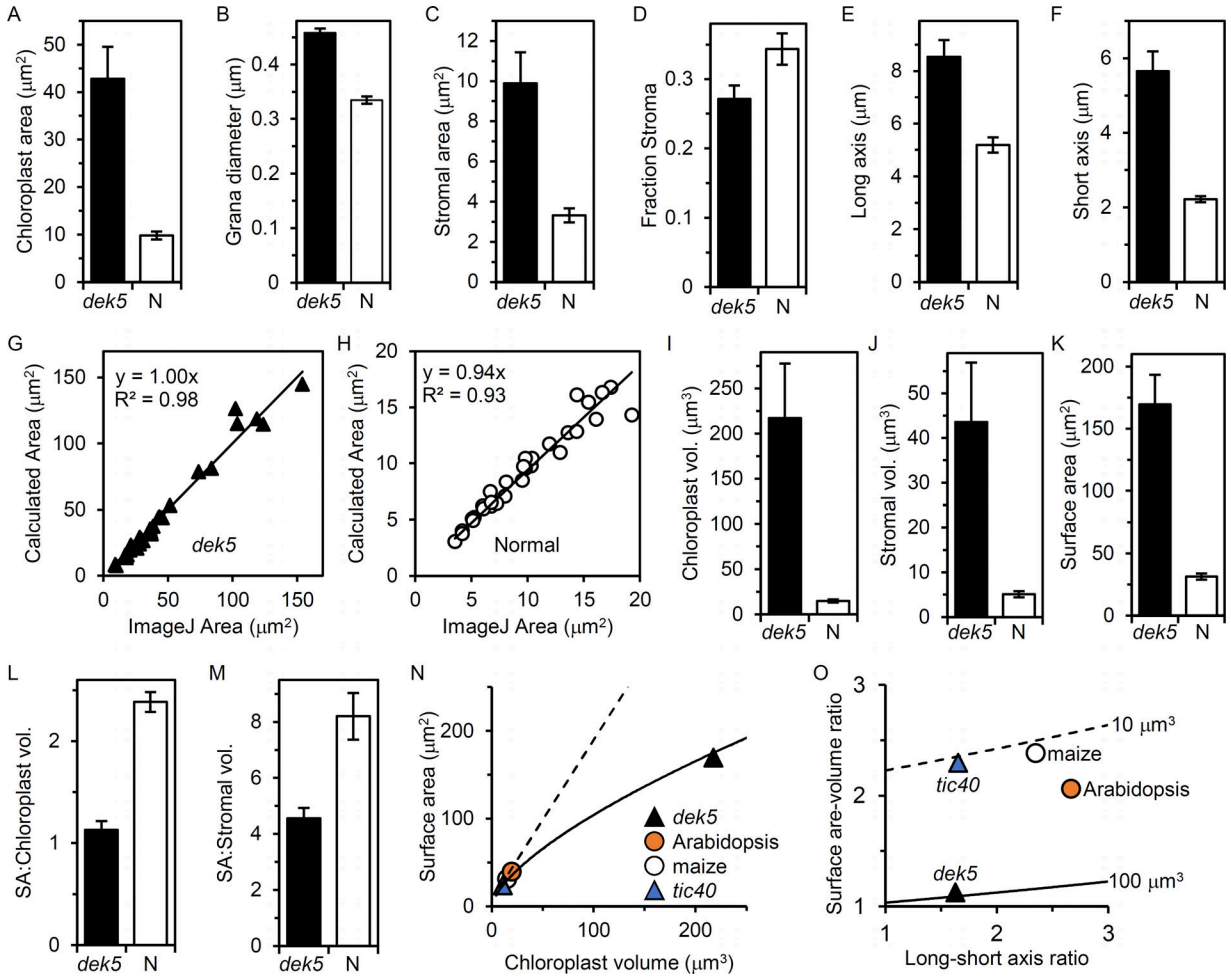

Figure 5. **Chloroplast traits based on TEM measurements. (A–F)** Traits quantified with ImageJ. Plots show mean and standard error (n = 31 [*dek5*] and 30 [normal (N)] chloroplasts). **(G and H)** Cross-sectional area calculated as an ellipse from long and short axes versus ImageJ measurements. Regression is with the y intercept set to zero. **(I–M)** Calculated traits from an ellipsoid using the long and short axes. SA, surface area. **(N and O)** Comparison of average traits for *dek5*, normal siblings (maize), the *A. thaliana tic40* mutant, and WT Columbia-O (*Arabidopsis*). *Arabidopsis* measurements are from Kovacheva et al. (2005). The dotted line in N is a cylinder with a 2.2 µm short axis. The solid line shows the relationship for a sphere. In O, lines show ellipsoid surface area/volume ratios as a function of aspect ratio for 10 µm³ (dotted) and 100 µm³ (solid) volumes. Graphs show mean and standard error (n = 31 [dek5] and 30 [normal (N)] chloroplasts).

(Selkrig et al., 2012). Phylogenetic analysis indicates that DEK5 has additional conserved sequence domains within land plants (Matsushima et al., 2014; Figs. 8 and S3).

DEK5 localizes to the chloroplast envelope

Chloroplast targeting of DEK5 was tested by fusing the 5′ 1,374 bp of the *Dek5* ORF with *EGFP* (Fig. 9, A and B; and Fig. S3). Transient expression of DEK5N-GFP in *Nicotiana benthamiana* leaves resulted in a punctate ring of GFP signal surrounding red chlorophyll fluorescence from thylakoid membranes (Fig. 9 B). This pattern is identical to known chloroplast envelope membrane proteins, such as CHUP1, OEP7, Tic40, and Tic20 (Oikawa et al., 2008; Breuers et al., 2012; Machettira et al., 2012). However, it contrasts with stromal localization reported for a differing length N-terminal fragment of SSG4 fused to GFP (Fig. S3; Matsushima et al., 2014).

Deletion of the predicted TMD sequence from DEK5N-GFP resulted in DEK5NΔTMD-GPF showing punctate distribution of GFP fluorescence overlapping with chlorophyll fluorescence, indicating targeting to plastids (Fig. 9 C). Fusing only the DEK5 TP and TMD was sufficient for envelope localization of GFP signal (Fig. 9 D). These results support the conclusion that the DEK5 TMD is necessary and sufficient for envelope localization.

Polyclonal antibodies raised against the DEK5 TamB domain cross-react with an ∼100-kD polypeptide that copurifies with WT chloroplasts as well as a larger band in total leaf protein (Figs. 9 E and S4 A). Preincubation of the α-DEK5 sera with the TamB recombinant antigen causes loss of the 100-kD signal, showing that this band is specific for the DEK5 protein despite migrating much faster than the full-length protein (Fig. S4 B). The *A. thaliana* TIC236 orthologue is easily degraded, suggesting the maize signal is a partially degraded protein (Chen et al., 2018). The specific α-DEK5 signal is reduced in *dek5* leaf extracts, and the amount of DEK5 protein correlates with the strength of the mutant phenotype (Figs. 9 E and S4 C). The severe *dek5-Briggs* and *dek5-N1339A* alleles have little to no

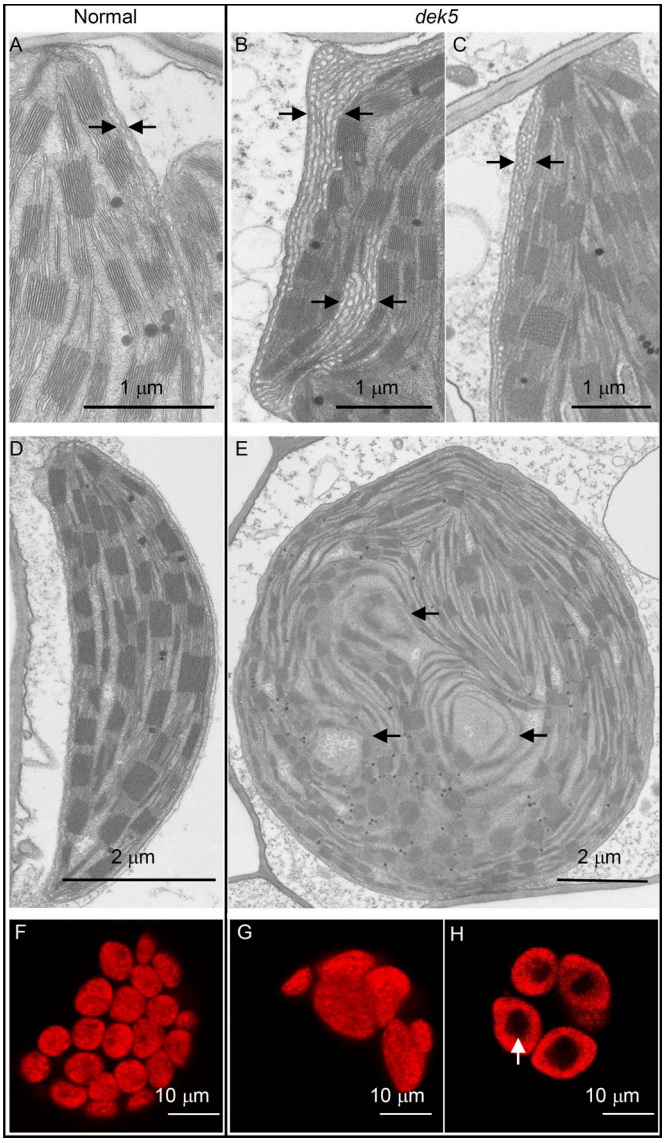

Figure 6. **Range of *dek5* chloroplast membrane defects. (A and D)** Normal mesophyll chloroplast. **(B and C)** Thick chloroplast reticulum (black arrows) in *dek5*. **(E)** Disorganized *dek5* thylakoids. **(F–H)** Individual laser confocal scanning microscopy cross sections of protoplast chlorophyll autofluorescence. **(F)** Normal sibling. **(G)** *dek5*, fully fluorescent chloroplasts. **(H)** *dek5*, central thylakoid fluorescence reduced (white arrow).

detectable DEK5 protein as well as severely reduced outer envelope (Toc75 and OEP80) and thylakoid (cytochrome f [Cyt f]) membrane proteins (Fig. S4 C). These data indicate that α-DEK5 reports a DEK5 protein that is most likely a C-terminal fragment without a TMD.

Chloroplasts fractions of soluble, thylakoid membrane, IEM, and outer envelope membrane (OEM) showed that DEK5 co-fractionated with envelopes and soluble proteins (Fig. 9 F). Compartment-specific protein markers have clean separation of soluble proteins from envelope membranes. The DEK5 membrane association can be disrupted by washes with 0.1 M Na_2CO_3 or 1 M NaCl, but not with 6 M urea (Fig. 9 G). The thylakoid membrane-associated oxygen evolving complex 23-kD (OEC23) subunit has similar sensitivity, while the integral membrane Cyt f protein is resistant to all salt and chaotropic agents. These data are consistent with a C-terminal degradation product of DEK5 lacking the TMD.

A dual-protease protection assay was used to determine the topology of DEK5 (Froehlich, 2011). Thermolysin only digests proteins on the outer face of the OEM. DEK5, 6PGDH, and OEP80 were all resistant to thermolysin when chloroplasts are intact (Fig. 9 H). Each of these proteins show some sensitivity to thermolysin when chloroplasts are lysed under hypotonic conditions. By contrast, trypsin digests protein domains in the intermembrane space between the OEM and IEM. The OEM protein OEP80 is sensitive to trypsin, while stromal 6PGDH is resistant (Fig. 9 I). DEK5 was partially digested by trypsin in five biological replicates (Figs. 9 I and S4 D). All three proteins are fully digested in hypotonic chloroplast lysates. These results suggest that DEK5 protein is sensitive to trypsin and likely to face the intermembrane space between the OEM and IEM. This is the topology of TamB in *E. coli* and TIC236 in *A. thaliana* but is contrasting to the stromal localization reported for rice SSG4 (Selkrig et al., 2012; Matsushima et al., 2014; Chen et al., 2018).

Chloroplast envelope protein composition is altered in *dek5*

DEK5 envelope localization and intermembrane space topology support an orthologous function to TamB in facilitating membrane protein insertion. Proteomics of purified chloroplast envelope fractions showed broad changes in envelope protein composition (Fig. 10 A). This analysis identified 68 known chloroplast envelope protein homologues. We compared envelope protein abundance by normalizing MaxQuant intensity values for the envelope proteins detected (Table S1). Nearly 33% of these proteins were reduced or absent in *dek5*. Among 22 proteins with reduced abundance, 91% are predicted to function in membrane transport.

Half of the OEM integral membrane proteins (5/10) were down-regulated in *dek5*, with the remaining OEM proteins being unchanged in relative abundance (Fig. 10 A). OEM proteins with reduced levels included the chloroplast protein targeting machinery, Toc34, Toc75, and Toc159, as well as OEP16 and OEP80. These results are consistent with immunoblots of *dek5* leaf protein showing that Toc75 and OEP80 are reduced (Fig. S4 C).

Seven membrane proteins had increased relative abundance in the IEM. However, 14 IEM proteins were reduced in *dek5*, including a Na^+-dependent P_i transporter and two P_i/phosphoenolpyruvate translocators (Table S1). Both α-helical and β-barrel transmembrane proteins are reduced in *dek5*, and we conclude that there are pleiotropic defects in envelope protein composition.

P_i uptake is compromised in *dek5* chloroplasts

Reduced P_i transporter levels in *dek5* envelopes suggest that P_i transport may be affected. P_i uptake was assayed by incubating purified chloroplasts with $^{32}P_i$ (Fig. 10 B). Normal chloroplasts reach equilibrium $^{32}P_i$ levels between 3 and 5 min in 0.1 mM P_i. Mutant *dek5-N961* chloroplasts show no appreciable uptake over the 5-min incubation at 0.1 mM P_i. Higher P_i concentrations of 0.5 mM (5×) or 10 mM (100×) did not increase uptake to normal

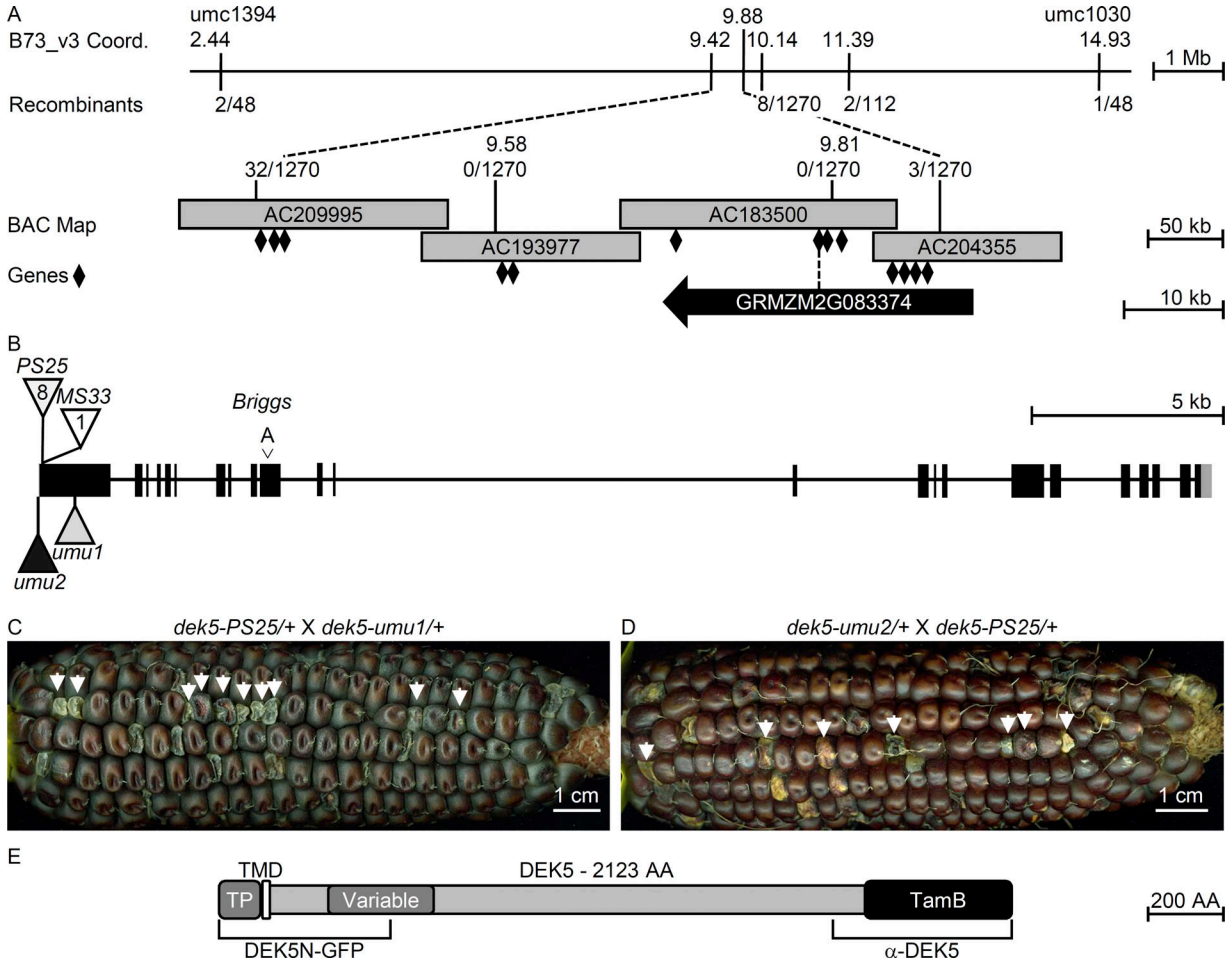

Figure 7. **Map-based cloning of the *Dek5* gene. (A)** Integrated physical-genetic map of the *dek5* locus. B73 AGP_v3 physical coordinates are given for molecular markers with recombinants/number of meiotic products genotyped. Bacterial artificial chromosome (BAC) sequences were aligned with blastn to determine overlap regions. Genes in the fine-map interval are denoted with triangles except for *dek5*, GRMZM2G083374. **(B)** *Dek5* locus schematic. Black boxes are coding exons, gray boxes are untranslated regions, and introns are lines. Triangles indicate *Mu* insertions with *dek5-PS25* having a *Mu8-like* insertion at the same site as *dek5-MS33* with a *Mu1* insertion. **(C)** Complementation test of *dek5-PS25* with UniformMu allele, mu1021358 (*dek5-umu1*). **(D)** Complementation test of *dek5-PS25* with UniformMu allele, mu1047944 (*dek5-umu2*). Arrows indicate noncomplementing mutants in a single row of kernels. **(E)** DEK5 protein domains: N-terminal TP, a single-pass α-helical TMD, and a C-terminal TamB domain. Brackets indicate regions for the C-terminal GFP fusion (DEK5N-GFP) and antibody production (α-DEK5).

levels. A longer incubation time at 0.5 mM P_i showed no appreciable uptake.

P_i accumulates in the stroma, and uptake is limited by total stromal volume (Fliege et al., 1978). A dilution series of normal chloroplasts found that the detection limit of $^{32}P_i$ uptake is ∼20–50% of the stromal volume in the standard assay (Fig. 10 C). Although *dek5* volume is larger than in normal chloroplasts, thylakoids account for ∼10% more of total chloroplast volume, leading to a relative reduction in stroma (Fig. 5 M). To normalize P_i uptake on stromal volume, we counted chloroplast number and estimated the average stroma volume. A dilution series from 1.7- to 5.8-fold larger stromal volume relative to the standard assay with normal chloroplasts showed no appreciable P_i uptake (Fig. 10 C). Based on the normal and *dek5* chloroplast dilution series, we expected to observe uptake if *dek5* membrane had as little as 17% of normal P_i uptake.

To control for chloroplast integrity throughout the assay, we completed P_i uptake assays without radioactive labeling and purified the chloroplasts in an isosmotic sorbitol solution. Phase-contrast microscopy of the recovered chloroplasts showed that *dek5* chloroplasts were intact (Fig. 10, D and E). Immunoblots of purified chloroplasts loaded on an equal chlorophyll content showed equivalent levels of thylakoid membrane proteins CF1-β and Cyt f, as expected for this normalization (Fig. 10 F). DEK5 and OEP80 proteins were reduced in the mutant chloroplasts relative to thylakoid membrane proteins. This result is consistent with TEM and proteomics observations, from which *dek5* and normal chloroplasts are predicted to have different amounts of envelope membrane relative to chlorophyll content or thylakoid membrane proteins. Together, the data argue that multiple envelope membrane proteins and P_i transport are greatly reduced in *dek5* chloroplasts.

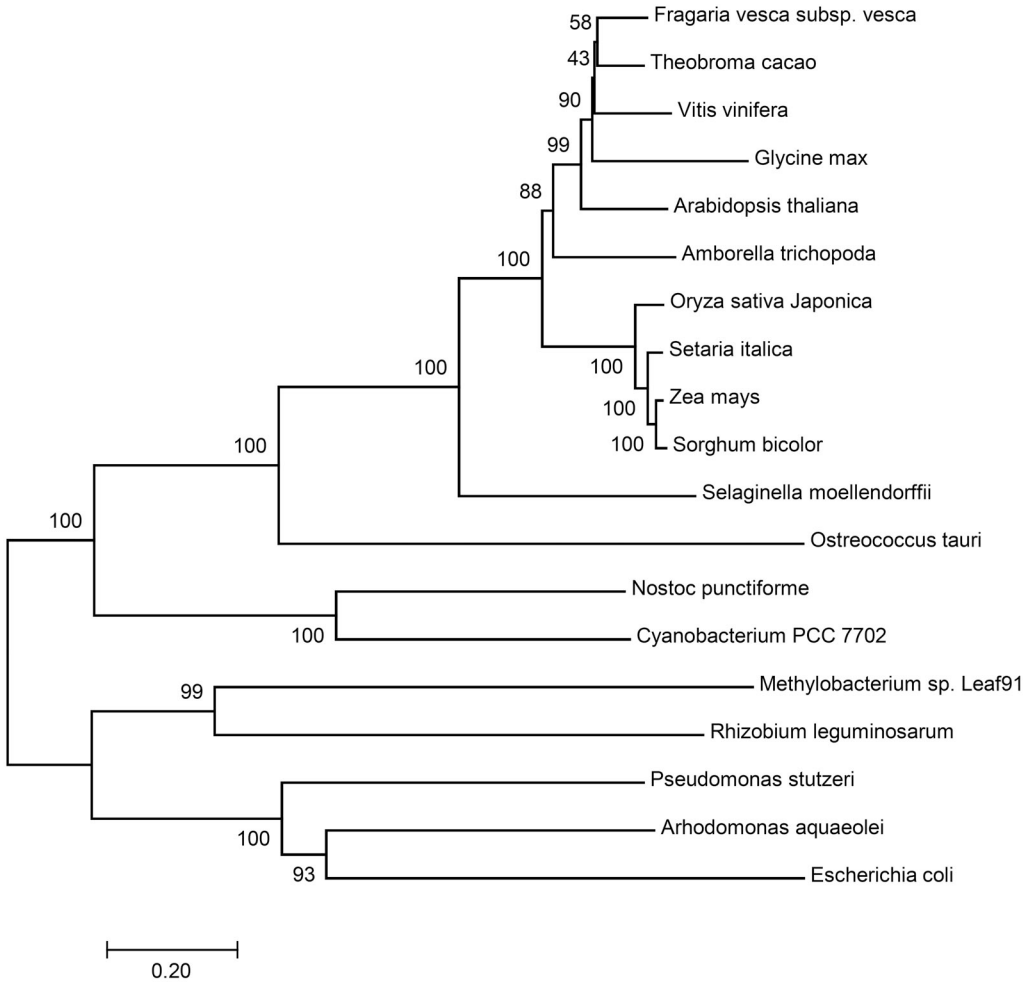

Figure 8. **Phylogenic analysis of DEK5 orthologous proteins.** Neighbor-joining phylogenetic tree constructed with MEGA 7. Bootstrap values are indicated at each node of the tree. Scale indicates genetic distance as amino acid changes per residue.

Discussion

Cloning of *dek5* revealed that the locus is orthologous to rice *ssg4* and *A. thaliana tic236* (Matsushima et al., 2014; Chen et al., 2018). However, we have come to different conclusions about the biochemical function of plant TamB proteins. Matsushima et al. (2014) suggested that SSG4 has a novel function in chloroplast division. Chen et al. (2018) suggested that TIC236 evolved a novel function in protein import. We propose that the DEK5/SSG4/TIC236 proteins have analogous envelope biogenesis roles to bacterial TamB proteins.

A series of alleles with differing severity is critical to develop an accurate the model for plant TamB homologues. The rice *ssg4* locus is defined by a single mutant allele with a missense mutation (Matsushima et al., 2014). Compared with *dek5*, *ssg4* shows mild starch granule and chloroplast phenotypes with no ultrastructural changes observed in plastid membranes. The severe alleles of *A. thaliana emb2410/tic236* arrest seed development at the globular embryo stage (Tzafrir et al., 2004). Weak *tic236* alleles cause leaf morphology defects, but chloroplast ultrastructure was not characterized (Chen et al., 2018). Maize alleles expressing some DEK5 protein give more normal development, while strong alleles lacking DEK5 protein cause severe seed defects and embryo lethality. Much of our phenotypic analysis focused on the mild *dek5-MS33* and *dek5-N961* alleles, which enable sufficient plastid development to observe a range of organelle defects. From these phenotype data, we conclude that *dek5* is required for envelope biogenesis and plastid metabolite transport.

DEK5 is required for plastid metabolite transport

Multiple lines of evidence suggest *dek5* disrupts intracellular metabolite transport. Sucrose is the carbon source for endosperm starch synthesis. Endosperm starch is decreased in *dek5* with concomitant increase of sucrose, suggesting that carbon is not limiting. Sucrose is converted to ADP-glucose in the cytoplasm of endosperm cells (Hannah, 1997). The BT1 inner envelope transporter selectively transports ADP-glucose into the amyloplast (Shannon et al., 1998). Like *bt1*, *dek5* mutants have higher levels of ADP-glucose, suggesting that reduced transport into amyloplasts may be the cause of increased sugars (Tobias et al., 1992; Shannon et al., 1996). This inference is further supported by nearly identical starch-branch chain lengths in

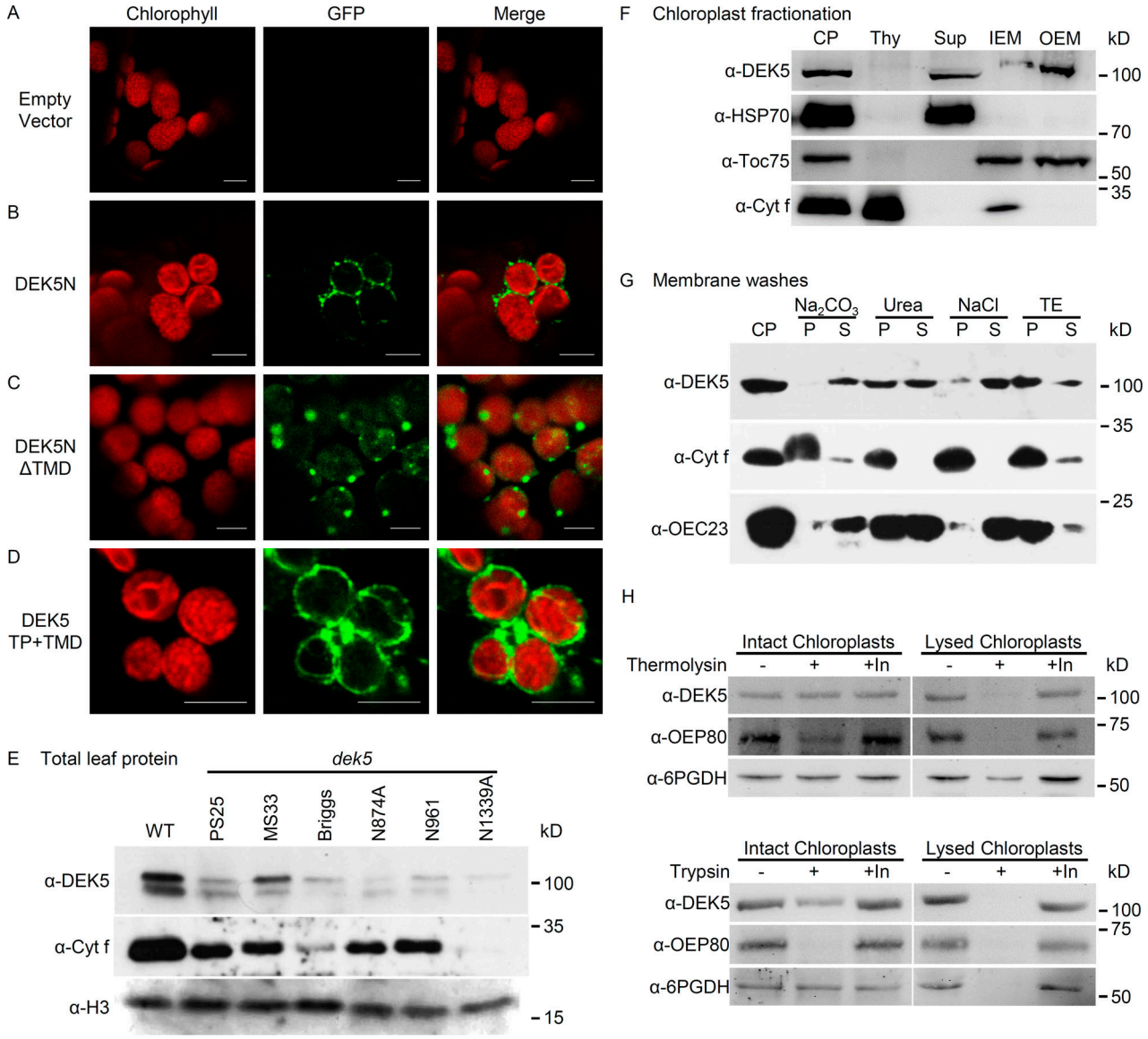

Figure 9. **DEK5 topology. (A–D)** Confocal micrographs after transient expression of GFP fusion proteins in *N. benthamiana* leaves. **(A)** Empty vector is pB7FWG2. **(B)** DEK5N-GFP has the N-terminal region shown in Fig. 7 E. **(C)** DEK5NΔTMD-GFP has an in-frame deletion of the predicted TMD. **(D)** DEK5TP+TMD-GFP includes on the predicted chloroplast targeting sequence and TMD. Scale bars are 5 µm in all panels. **(E)** Immunoblots of total leaf protein with antibodies detecting DEK5, Cyt f, and H3 proteins. **(F)** Subfractionation of isolated whole chloroplasts (CP) into thylakoid (Thy), soluble (Sup), IEM, and OEM fractions. HSP70 is a soluble, stromal protein. **(G)** Washes of isolated chloroplasts using chaotropic agents or freeze–thaw lysis (TE). Immunoblots have membrane pellets (P) and soluble (S) fractions. OEC23 is a peripheral thylakoid membrane protein. **(H and I)** Protease protection assays with purified chloroplasts treated with thermolysin (H) or trypsin (I) proteases (+) or the protease plus protease inhibitors (+In).

dek5 and normal endosperm starch, indicating normal polymerization and debranching within the amyloplast.

There is also evidence for solute transport defects in *dek5* leaves. Maize fixes CO_2 in mesophyll chloroplasts and shuttles malate into bundle sheath chloroplasts for starch synthesis (Majeran et al., 2005; Weise et al., 2011). TEM of *dek5* bundle sheath chloroplasts found few starch granules but extensive thylakoid vesicular structures consistent with an osmotic imbalance between the chloroplast and cytosol. Moreover, *dek5* mesophyll chloroplasts accumulate starch, potentially indicating reduced flux of malate from the mesophyll.

Proteomics found reduced metabolite and ion transporters in *dek5* envelopes. P_i uptake was not detected for *dek5* chloroplasts in vitro. The sensitivity of the assay indicates that *dek5* chloroplasts have ±80% reduction in P_i transport. These data support a role for DEK5 in envelope protein accumulation and metabolite transport. Transport of exogenous ATP into purified chloroplasts is required for efficient in vitro chloroplast import (Theg et al., 1989). Although we did not specifically measure ATP uptake, reduced transport could explain reduced protein import efficiency observed for *tic236* mutants (Chen et al., 2018).

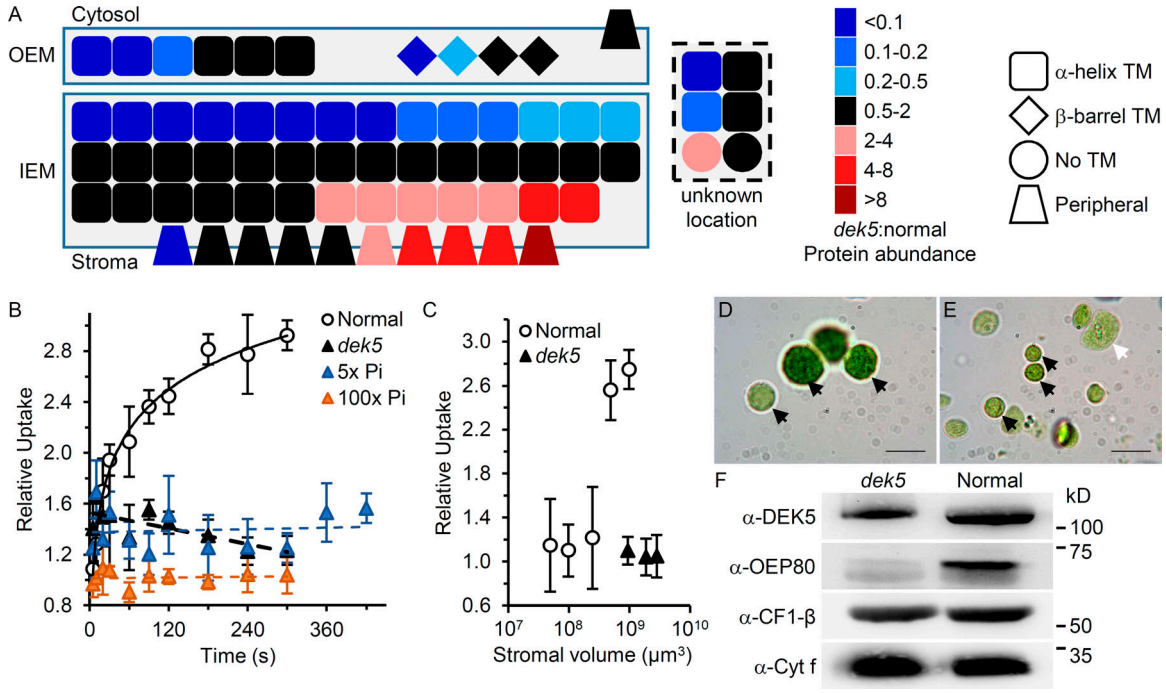

Figure 10. **Defective *dek5* chloroplast envelope membranes. (A)** Relative levels of *dek5* to normal chloroplast envelope proteins. Symbols indicate the type of TMD predicted for each protein. Proteins in the dotted box have only been localized to envelope membranes. **(B)** Time course of $^{32}P_i$ uptake in isolated normal and *dek5-N961* chloroplasts. Mean and standard deviation are plotted (n = 3 biological replicates). **(C)** End-point $^{32}P_i$ uptake of normal and *dek5-N961* chloroplast dilutions after a 5-min incubation. Mean and standard deviation are plotted (n = 3 biological replicates). Total stromal volume was estimated based on the number of chloroplasts included in each assay. **(D and E)** Phase-contrast micrographs of *dek5-N961* (D) and normal (E) chloroplasts after a mock P_i uptake assay. Black arrows indicate intact chloroplasts. The white arrow indicates a broken chloroplast. Scale bars are 10 µm. **(F)** Immunoblot analysis of purified *dek5-N961* and normal sibling chloroplasts. Protein was loaded on an equal OD_{652} basis.

DEK5 is required for chloroplast membrane biogenesis

Proteomics and P_i uptake data are consistent with *dek5* chloroplast size and ultrastructure. Mutant chloroplasts have much larger chloroplasts, but envelope surface area is reduced relative to volume. *A. thaliana* chloroplast division mutants have fewer and larger chloroplasts but do not limit envelope membrane biogenesis (Pyke and Leech, 1992; Pyke et al., 1994; Robertson et al., 1996; Shimada et al., 2004; Maple et al., 2007). TEM of division mutants shows elongated chloroplasts that maintain a surface area to volume ratio closer to WT.

The peripheral reticulum is also expanded in *dek5*, which is a tubular network derived from the inner envelope (Wise, 2007). This ultrastructural change may indicate differential development of inner and outer envelopes analogous to a mutation in a TamB homologue, morC, in *Aggregatibacter actinomycetemcomitans*. The morC mutation reduces outer membrane relative to inner membrane, resulting in a smooth surface, when WT cells have convoluted, rugose outer membranes (Gallant et al., 2008; Azari et al., 2013). Like *dek5* chloroplasts, morC mutants have a more spherical cell morphology, suggesting that loss of TamB function can lead to similar membrane imbalance in both bacteria and chloroplasts.

TamB mutants in *E. coli*, *A. actinomycetemcomitans*, and *Deinococcus radiodurans* all disrupt localization of a subset of outer membrane proteins (Selkrig et al., 2012; Azari et al., 2013; Shen et al., 2014; Yu et al., 2017). In the *dek5* outer envelope, half of the membrane proteins are reduced, while a subset of inner envelope protein have increased relative levels. This observation argues that the outer envelope is more compromised in *dek5* relative to the inner envelope.

Thylakoids can also be disrupted in *dek5*, but the loss of thylakoid organization is likely secondary to defects in envelope proteins. Toc34, Toc75, and Toc159 are the core protein translocation complex (Schleiff et al., 2003; Baldwin et al., 2005). Based on proteomics, all three of these proteins have reduced levels in *dek5* envelopes. Toc75 levels in immunoblots correlate with the amount of DEK5 protein in the *dek5* allelic series. Toc75 is a β-barrel integral membrane protein that is the channel for translocation of nuclear-encoded proteins into the chloroplast (reviewed in Bölter and Soll, 2016). Loss of Toc75 in *A. thaliana* causes early embryo arrest, while knockdown reduces protein import, chloroplast size, and thylakoid development (Schleiff et al., 2003; Hust and Gutensohn, 2006). Variations in import machinery levels in *dek5* is expected to limit chloroplast protein accumulation and cause defects in thylakoid membranes.

The function of TamB in bacteria is to promote integration of β-barrel membrane proteins, including Omp85 family members like Toc75 (Selkrig et al., 2012; Shen et al., 2014; Yu et al., 2017). In *E. coli*, TamB interacts with TamA, the BAM subunits, and client proteins (Babu et al., 2018). The *A. thaliana* DEK5 orthologue, TIC236, interacts with Toc75, and weak *tic236* alleles reduce in vitro protein import (Chen et al., 2018). The *tic236* mutant did not impact Toc75 protein levels, and TIC236 was interpreted as having a direct role in import. Based on this

postulated role, *tic236* chloroplasts should be reduced in size, similar to a knockdown of *toc75*. Chloroplast structure was not investigated in *tic236*, but both *ssg4* and *dek5* show greatly enlarged chloroplasts, robust thylakoid development, and a relative reduction in envelope. These chloroplast phenotypes are opposite to predicted for a protein import mutant. We propose it is more likely that DEK5 plays a direct role in targeting β-barrel membrane proteins to the outer envelope.

DEK5 topology is analogous to TamB

Biochemical analysis of DEK5 topology further supports the model that plant TamB proteins have an analogous function with bacterial homologues. TamB is an inner plasma membrane protein that bridges the periplasmic space with an N-terminal TMD and a C-terminal TamB domain (Selkrig et al., 2012; Shen et al., 2014). Plant TamB proteins are much bigger than homologous proteins in proteobacteria. Matsushima et al. (2014) proposed that SSG4 has a distinct biochemical function from TamB, in part, based on protein length differences. However, Gram-negative bacteria have a 2–6-nm periplasm, while cyanobacteria and chloroplasts have thicker periplasm and intermembrane spaces of 10–35 nm (Hoiczyk and Hansel, 2000). Plant DEK5 proteins would need to be larger to bridge the intermembrane space of the plastid.

We used two experimental approaches to investigate DEK5 topology. An N-terminal region of DEK5 fused to GFP encompasses chlorophyll fluorescence identical to other envelope proteins (Okawa et al., 2008; Singh et al., 2008; Kasmati et al., 2011). Antibodies that cross-react with the C-terminal region of DEK5 support a model in which DEK5 is an intermembrane space protein associated with both outer and inner envelopes. This is the same topology as observed for *E. coli* TamB and TIC236 (Selkrig et al., 2012; Shen et al., 2014; Chen et al., 2018).

A revised model for plant TamB homologues

Reconciling all available data for plant TamB proteins argues for a function in chloroplast envelope biogenesis. Based on TamB function, we propose that DEK5, SSG4, and TIC236 have conserved roles in targeting a subset of β-barrel proteins to the outer envelope. The proteomics experiment identified Toc75 and OEP80 as likely client proteins. OEP37 levels were just above the twofold reduction cutoff in the proteomics analysis and may also be a DEK5 client. The correlation between the levels of chloroplast import machinery and the severity of *dek5* mutant alleles suggests that severe alleles display extreme pleiotropy with plastids being unable to support import of nuclear-encoded proteins. Weak alleles that support protein import would also retain sufficient DEK5 activity to support β-barrel protein insertion. Consequently, direct proof of the proposed functions in OEP insertion or protein import will require biochemical methods to block DEK5 action in WT chloroplasts.

Materials and methods

Plant materials

All maize plants were grown during April–July or August–December at the University of Florida Institute of Food and Agricultural Sciences Plant Science Research and Education Unit in Citra, Florida. The *dek5* and normal siblings were germinated in a greenhouse with Metro-Mix 300 (Scotts-Sierra). The *dek5-N874A*, *dek5-N961*, and *dek5-N1339A* alleles were originally isolated by Neuffer and Sheridan (1980) from ethyl methanesulfonate mutagenesis. Scanlon et al. (1994) isolated *dek5-PS25* and *dek5-MS33* from *Mutator* transposon-tagging populations. The *dek5-Briggs* allele is a spontaneous mutation (www.maizegdb.org). Stocks for *dek5* alleles were ordered from the Maize Genetics COOP Stock Center. Each *dek5* allele was crossed with B73, W22, or Mo17 inbred lines five times to develop BC_4 introgression stocks to characterize phenotypes. The *dek5-umu1* (mu1021358) and *dek5-umu2* (mu1047944) UniformMu alleles were maintained in the W22 inbred background. We confirmed all stocks were *dek5* alleles by genetic complementation tests using reciprocal crosses between each stock and *dek5-PS25*. First ears were used for reciprocal crosses. Second ears of both male parents and female parents in the crosses were self-pollinated to determine plant genotypes.

Endosperm composition analysis

Endosperm composition was determined from dissected tissues. Developing endosperm was flash frozen in liquid nitrogen and stored at −80°C. Frozen endosperm tissues were cracked into small pieces with mortar and pestle, lyophilized for 3 d, and ground to a fine powder with a bead mill. For mature dry kernels, endosperm was isolated by cutting the kernel in the sagittal plane and cutting away the embryo with a utility knife. The pericarp was removed by scraping the surface of the mature dry endosperm with a razor blade. The remaining endosperm tissue was ground to a fine powder with a bead mill.

Zein and nonzein protein was extracted from the dissected, dry endosperm tissue as described by Wu and Messing (2012). Protein extracts were loaded on equal dry weight basis for SDS-PAGE and stained with Coomassie Blue R-250. Endosperm starch was measured from developing kernels using the Megazyme Total Starch Assay Kit (AA/AMG). Sucrose, glucose, and maltose were measured with the Megazyme Maltose/Sucrose/D-Glucose Assay Kit (K-MASUG). ADP-glucose was measured with a glycerol-3-phosphate oxidase/glycerol-3-phosphate dehydrogenase cycling assay as described previously (Gibon et al., 2002). Briefly, frozen endosperm was ground and extracted in 200 mM tricine/KOH, pH 8, containing 10 mM $MgCl_2$. 30 µl of endosperm extracts or ADP-glucose standards (0–20 pmol) was dispensed into a microplate with 20 µl tricine buffer containing 0.05 U UGPase, 0.05 U glycerokinase, 2.5 U Gly3POX, 130 U catalase, 0.05 U triose phosphate isomerase, 0.1 U GAPDH, 0.02 µmol P P_i, 0.15 µmol NaF, 0.25 µmol glycerol, 0.01 µmol NAD^+, and 0.1 µmol sodium arsenate. Reactions were incubated for 40 min at room temperature, and 20 µl of 1.2 mM NADH solution containing 0.4 U glycerol-3-phosphate dehydrogenase was added. Absorbance at 340 nm was recorded over 20 min. Next, 0.3 U AGPase was added, and the absorbance read 340 nm for 20 min. The difference in the two rates was used to calculate the amount of ADP-glucose in the sample.

Starch analysis

Developing kernels were collected and fixed in FAA solution (3.7% formaldehyde, 5% glacial acetic acid, and 45% ethanol) at 4°C overnight. Kernels were dehydrated in an ethanol series and kept in 100% ethanol. Additional sample preparation and scanning EM observations were performed at Interdisciplinary Center for Biotechnology Research Electron Microscopy core at the University of Florida, Gainesville, FL. Scanning EM data were collected with a Hitachi SU5000 Schottky field emission scanning electron microscope. Starch granule diameter was measured using ImageJ for three scanning EM images from each genotype and developmental stage. For particle size analysis, mature endosperm tissue was dissected and ground into fine powder with a bead mill. Endosperm powder (0.1 g) was mixed with 1 ml of ethanol and vortexed immediately before measurement with a Beckman/Coulter LS 13 320 laser diffraction particle size analyzer.

Amylopectin chain length distribution of endosperm starch

Single endosperms were homogenized on ice in a mortar and pestle in 4 ml H_2O. Starch from 1 ml lysate was pelleted in a 2-ml polypropylene tube by centrifugation at 1,400 *g* for 10 min at 4°C. The starch pellet was washed twice in ice cold 80% ethanol with centrifugation at 1,400 *g* for 5 min. Starch was dissolved by boiling in 1 ml DMSO for 20 min and then quantified by enzymatic conversion to glucose (Lin et al., 2012; Huang et al., 2014). For the debranching reaction, 1.5 mg of dissolved starch polymers was precipitated with 5 vol of ethanol at −20°C for ≥1 h. Glucans were collected by centrifugation at full speed in a microfuge at room temperature and then suspended in 0.5 ml 50 mM sodium acetate, pH 4.5, containing 0.05 U *Pseudomonas* isoamylase (Megazyme no. E-ISAMY) and incubated overnight at 50°C. The solution was then diluted with 1.5 ml H_2O, filtered through a 0.2-µm syringe-tip filter, and 25 µl was applied to a high-pressure ion-exchange chromatography system with pulsed amperometric detection (HPAEC-PAD) that resolves and quantifies α(1→4)-linked (linear) glucan chains ranging from 2 to 40 glucosyl units. Separation was on a Dionex CarboPac PA-100 4 × 250–mm column with a CarboPac PA-100 4 × 50–mm guard column at a flow rate of 1 ml/min. Elution was in 0.1 M NaOH for 4 min followed by a 40-min gradient of 0–0.4 M sodium acetate in 0.1 M NaOH. Peak areas for each degree of polymerization (DP) were normalized to the total peak area, and the normalized values for each DP were compared between samples.

Protoplast analysis

Maize protoplasts were prepared essentially as described previously (Yoo et al., 2007), with some modifications. Kernels were planted in a greenhouse. After 10 d, 0.5 g seedling leaves was harvested, chopped with a razor blade, and digested in enzyme solution at 28°C for 4–5 h with a gentle shaking at 60 rpm in the dark. The enzyme solution consisted of 1.5% (wt/vol) cellulase R10, 0.5% (wt/vol) macerozyme R10 in 0.4 M mannitol, 20 mM KCl, 10 mM $CaCl_2$, 5 mM β-mercaptoethanol, 0.1% BSA, and 20 mM MES, pH 5.7. Cell debris was filtered using 35-µm nylon mesh, and collected protoplasts were suspended in W5 solution (2 mM MES, pH 5.7, 154 mM NaCl, 125 mM $CaCl_2$, and 5 mM KCl) and kept on ice for observation. Protoplast isolation at high osmotic concentration replaced 0.4 M mannitol with 0.8 M mannitol in all solutions. Protoplast yield was determined by counting intact protoplasts in W5 solution using a hemocytometer and a Zeiss Standard WL microscope with a Neofluor 40×/0.75 objective at room temperature. Light microscopy imaging used an AMScope MU500 digital camera with the AMscope acquisition software version 3.7 for a Windows 64-bit operating system.

Chloroplast number within each cell was determined with Z-stack images of individual protoplast cells using a Leica TCS SP5 laser-scanning confocal microscope (Leica Microsystems). Images were captured at 37°C using a 100× PL APO NA 1.40 oil-immersion objective (Leica) and a filter cube set for FITC/TRITC for multicolor fluorescence. Leica LAS AF software was used to acquire images with water as the imaging medium. Chlorophyll was excited at 488 nm and detected with an emission band of 650–700 nm. A 3D image was reconstructed for each cell and manually scored for the number of chloroplasts. Chloroplast cross-sectional surface areas and volume were measured using ImageJ (Schindelin et al., 2012).

Leaf pigment extraction and measurement

Fresh seedling leaf tissue (0.5 g) from both *dek5* mutant and normal siblings was harvested and chopped with a razor blade. The leaf tissue was extracted in 15 ml of 96% ethanol with gentle agitation for 12 h at room temperature in aluminum foil wrapped bottles. Ethanol extracts were separated from tissue debris with filter paper. The tissue was rinsed with 96% ethanol to completely extract residual pigment. The extract and rinse were combined and brought to 25 ml final volume in 96% ethanol. Chlorophyll a, chlorophyll b, and carotenoid absorbance was measured at 665, 649, and 470 nm using a spectrophotometer. Pigment content was calculated according to Lichtenthaler and Wellburn (1983).

Immunoblotting

Chloroplast protein or total seedling proteins were separated by 10% SDS-PAGE and transferred to nitrocellulose membrane using a Bio-Rad Trans-Blot SD semi-dry transfer cell at 15 V for 30 min. Membrane was first blocked with blocking solution containing 3% BSA and 0.2% Tween 20 with PBS (pH 7.4) at room temperature for 30 min and then incubated with primary antibody at 1:2,000 dilution in blocking solution for 2 h at room temperature or overnight at 4°C. Membranes were washed four times for 5 min using PBS with 0.2% Tween 20. Primary antibody signal was detected after incubating goat anti-rabbit secondary antibody (Sigma) at 1:1,000 dilution in blocking solution for 2 h at room temperature followed by four 5-min washes using PBS with 0.2% Tween 20. Chemiluminescent was produced by applying 1 ml ECL substrate (Thermo Scientific Pierce) per gel membrane and imaging with a FOTODYNE FOTO Luminary/FX digital imaging system.

Leaf TEM

Seedling leaf tissues were harvested 10 DAS in a growth chamber. Sample fixation, sectioning and TEM were completed by

Electron Microscopy Services, as described previously (Turgeon and Medville, 2004). Briefly, leaf samples were fixed for 4 h at 4°C in 2% (wt/vol) paraformaldehyde and 2.5% (vol/vol) glutaraldehyde in 70 mM sodium cacodylate buffer, pH 6.8, followed by overnight incubation in 1% (wt/vol) osmium tetroxide in fixation buffer. Fixed tissues were subsequently dehydrated and embedded in resin. Ultrathin sections were stained with uranyl acetate and lead citrate for observations at 60 kV with a Philips EM-300 transmission electron microscope.

Chloroplast cross-sectional surface areas and volume measurements

Chloroplast area, long (a) axis, and short (b) axis were measured in ImageJ from TEM images using freehand selections for area and straight line selections for axes (Schindelin et al., 2012). Estimated cross-sectional area was calculated using the formula for an ellipse ($A = \pi ab$). Stroma and thylakoid areas were estimated by first determining the average auto threshold value for all TEM images. The average threshold value was applied to all images to measure thylakoid area, which was subtracted from chloroplast area to estimate stroma area. Calculations for ellipsoid volume,

$$V = \frac{4}{3}\pi ab^2,$$

and surface area,

$$S \approx 4\pi\left[\frac{2a^p b^p + b^p b^p}{3}\right]^{1/p}$$

(P = 1.6075), assumed the chloroplast long (a) axis represents length and the short (b) axis represents height and width. Thylakoid and stroma volumes were calculated for each chloroplast based on the relative fraction of the total chloroplast area. All traits were calculated for each chloroplast individually with mean and standard deviation statistics calculated using the estimated traits. Models for a cylinder volume,

$$V = \pi\left(\frac{b}{2}\right)^2 a,$$

and surface area,

$$A = 2\pi\left(\frac{b}{2}\right)^2 a + 2\pi\left(\frac{b}{2}\right)^2,$$

assumed the chloroplast long (a) axis was the height and the short (b) axis was the diameter. Models for a sphere volume,

$$V = \frac{4}{3}\pi r^3,$$

and surface area,

$$A = 4\pi r^2,$$

assumed a single radius (r).

Molecular identification of the *dek5* locus

An F_2 mapping population was generated by self-pollinating F_1 plants from a cross of the Mo17 inbred and *dek5-PS25/+*. Genomic DNA was extracted from individual F_2 mutant kernels and analyzed with simple sequence repeat and insertion-deletion PCR markers as described previously (Settles et al., 2014). Table S2 gives primer sequences of the markers used for linkage analysis. For the transposon flanking sequence experiment, homozygous *dek5-PS25* and *dek5-MS33* mutant genomic DNA was isolated from pools of six F_2 mutant kernels. *Mu* flanking sequences were amplified, purified, and adapted to the Illumina sequencing platform as described previously (McCarty et al., 2013). Reads were quality filtered and mapped to the B73_v3 genome assembly using the UniformMu informatics pipeline (McCarty et al., 2013).

RNA isolation and RT-PCR

Total RNA was isolated using Trizol (Invitrogen) from 10 DAS B73 maize seedlings. Approximately 1 mg of total RNA was reverse transcribed with either ThermoScript Reverse transcription (Invitrogen) for Dek5 cDNA cloning. Both oligo (dT) and random hexamer primers were used for first-strand synthesis to ensure full-length coverage of the *Dek5* mRNA. The *Dek5* cDNA was amplified with Phusion high-fidelity DNA polymerase (New England Biolabs) and cloned into pENTR/D-TOPO Vector (Invitrogen) as three overlapping fragments: *Dek5*-FN (1802 bp), *Dek5*-FM (2330 bp), and *Dek5*-FC (3006 bp). The full-length *Dek5* cDNA was assembled from the sequence of these clones. Specific PCR primers are listed in Table S2.

Phylogenetic analysis

Protein sequences were aligned using ClustalW (Larkin et al., 2007). The phylogenetic tree was produced with MEGA7 using the neighbor-joining method with 2,000 bootstrap replications and the Poisson substitution model (Hedges, 1992). The DEK5 homologue sequences used for phylogenetic analysis were *Zea mays* (GenBank accession no. MF034077), *Sorghum bicolor* (UniGene accession no. XP_002457235.1), *Glycine max* (NCBI Protein accession no. XP_003527803.1), *Oryza sativa Japonica* (Protein accession no. XP_015619226.1), *Setaria italic* (Protein accession no. XP_004971719.1), *Fragaria vesca subsp. Vesca* (Protein accession no. XP_011459147.1), *Vitis vinifera* (Protein accession no. XP_010648561.1), *A. thaliana* (Protein accession no. NP_180137.3), *Theobroma cacao* (GenBank accession no. EOY31352.1), *Amborella trichopoda* (Protein accession no. XP_006844393.1), *Selaginella moellendorffii* (Protein accession no. XP_002982313.1), *Ostreococcus tauri* (Protein accession no. XP_003079877.1), *Nostoc punctiforme* (Protein accession no. WP_012412249.1), *Cyanobacterium PCC 7702* (Protein accession no. WP_017320409.1), *Pseudomonas stutzeri* (Protein accession no. WP_003289734.1), *Methylobacterium sp. Leaf91* (Protein accession no. WP_082490488.1), *Rhizobium leguminosarum* (Protein accession no. WP_003543422.1), *Arhodomonas aquaeolei* (Protein accession no. WP_018716326.1), and *E. coli* (Protein accession no. WP_040089969.1).

Subcellular localization of DEK5

The DEK5N-GFP fusion protein was constructed by amplifying the initial 1,374 bp of the *Dek5* ORF from B73 seedling cDNA using Phusion high-fidelity DNA polymerase (New England Biolabs)

with the *Dek5*N-L and *Dek5*N-R primers (Table S2). The N-terminal ORF product was cloned into pENTR vector (Invitrogen) and recombined into the binary vector, pB7FWG2, to generate a C-terminal GFP fusion (Karimi et al., 2002, 2007). The TMD deletion was generated with the Q5 Site-Directed Mutagenesis Kit (New England Biolabs) to delete the peptide sequence, LFLVRCSVFAAVVSVAGALSW, in-frame from the DEK5N clone and then recombined into pB7FWG2. The binary constructs were transformed into *Agrobacterium tumefaciens* strain GV3101 by the freeze–thaw method (Weigel and Glazebrook, 2006). Each construct was transferred to *N. benthamiana* leaves via agroinfiltration as described previously (van Esse, 2012), with some modifications. Before infiltration, the agrobacteria were suspended in buffer containing 10 mM $MgCl_2$, 10 mM MES, and 200 µM acetosyringone and adjusted to an OD_{600} of 0.4. The *N. benthamiana* plants were grown in a growth chamber at 23°C with 16-h/8-h day/night light cycle. Leaves from 4–5-wk-old plants were infiltrated and examined by epifluorescence microscopy between 40 and 50 h after infiltration. Representative images were captured at 37°C using a 100× PL APO 1.40-NA oil-immersion objective (Leica) on an inverted Leica SP5 microscope equipped with a filter cube set for FITC/TRITC for multicolor fluorescence. Leica LAS AF software was used to acquire images with water as the imaging medium. GFP was excited at 488 nm and detected with an emission band of 500–530 nm. Chlorophyll was detected with an emission band of 650–700 nm. Captured images were processed with ImageJ to add scale bars to split and merged color channels.

Antibodies

The coding sequence for the DEK5 TamB domain was amplified with Phusion high fidelity DNA polymerase from B73 cDNA with the DUF490-L and DUF490-R primers (Table S2). The PCR product was digested with NcoI and NotI, purified, and cloned into the pMAL-c5X vector (New England Biolabs). Recombinant protein was expressed in the *E. coli* Top10 strain by inducing 12 liters of culture with 10 mM IPTG for 1 h at 30°C. Cells were sonicated using a 5-s/5-s pulse/pause cycle for a total of 3 min in an ice water bath. Recombinant protein was purified using amylose resin according to the manufacturer's instructions (New England Biolabs). The recombinant protein was concentrated in Amicon Ultra-15 Centrifugal Filters (EMD Millipore), and 2.5 mg of purified recombinant protein was sent to Thermo Scientific Pierce for rabbit polyclonal antibody production.

Other marker proteins were detected with rabbit polyclonal antibody sera raised against human histone H3 C-terminal peptide (ab1791; Abcam), spinach ATP synthase CF1-β (Fristedt et al., 2014), *A. thaliana* 6PGDH (Hölscher et al., 2016), sorghum OEC23 (Voelker and Barkan, 1995), maize Cyt f (Barkan et al., 1986), *A. thaliana* Toc75 (Ma et al., 1996), and *A. thaliana* OEP80 (Inoue and Potter, 2004).

Chloroplast isolation

Normal chloroplasts were isolated essentially as described previously (Voelker and Barkan, 1995). Leaf tissue from 7-d-old plants was cut and homogenized in grinding buffer (50 mM Hepes/KOH, pH 7.5, 0.33 M sorbitol, 1 mM $MgCl_2$, 1 mM $MnCl_2$, 2 mM EDTA, 5 mM Na-ascorbate, and 1% BSA) using a Warring blender with five bursts of ∼5 s at max speed. The homogenate was filtered through two layers of Miracloth, and the filtrate was centrifuged at 3,000 *g* for 5 min in a swinging bucket rotor at 4°C. The organelle pellet was gently suspended in 5 ml grinding buffer and layered onto a 35%/75% (8 ml/16 ml) Percoll step gradient. The gradient was centrifuged at 6,000 *g* for 15 min, and the lower, intact chloroplast, band was recovered. Intact chloroplasts were washed with import buffer (0.33 M sorbitol and 50 mM Hepes-KOH, pH 8.0) and pelleted by centrifugation at 1,000 *g* for 5 min. Pelleted chloroplasts were suspended in import buffer and adjusted to 0.5–1.0 mg chlorophyll per ml based on OD_{652}.

Mutant *dek5* chloroplasts were purified from protoplasts. Isolated *dek5* mutant protoplasts were washed and suspended in a protoplast hypotonic lysis buffer of 0.7 M sorbitol supplemented with 50 mM Hepes-KOH (pH 7.5). The cell lysate was passed through a 15-µm nylon mesh filter (Tisch Scientific) to further lyse remaining intact protoplasts. Released *dek5* mutant chloroplasts were purified in a 25%/75% Percoll step gradient centrifuged at 6,000 *g* for 15 min, and the lower, intact chloroplast band, was recovered. Isolated *dek5* chloroplasts were washed with 0.7 M sorbitol and 50 mM Hepes-KOH, pH 7.5, pelleted, and adjusted to 0.5–1 mg/ml chlorophyll.

Chloroplast fractionation

Chloroplasts were fractionated as described by Smith et al. (2003), with some modifications. Briefly, intact isolated chloroplasts were pelleted from import buffer and resuspended to 1–2 mg/ml chlorophyll in TE buffer (10 mM tricine and 2 mM EDTA, pH 7.5) with 0.6 M sucrose. Chloroplasts were lysed with two cycles of freezing and thawing and then diluted with TE buffer containing protease inhibitor cocktail (P9599; Sigma) to 0.2 M sucrose. Lysed chloroplasts were centrifuged at 45,000 *g* for 60 min to collect the crude envelope membranes. The soluble supernatant was collected and stored at −80°C for further analysis. The membrane pellet was resuspended in TE buffer containing 0.2 M sucrose to a concentration of 2–3 mg/ml chlorophyll, and 1 ml of the membrane suspension was layered onto the top of a sucrose gradient. The gradient consisted of 1.5 ml of 1 M sucrose, 1 ml of 0.8 M sucrose, and 1 ml of 0.46 M sucrose in a 5-ml polyallomer tube. The gradient was centrifuged for 1.5 h at 270,000 *g* at 4°C using low acceleration and deceleration rates. The yellow-green band from the 0.8 to 1 M sucrose interface was collected as the IEM fraction. The light yellow band from the 0.46–0.8 M sucrose interface was collected as the OEM faction. The green thylakoid pellet was resuspended in TE. All membrane fractions were washed using 3–5 vol of TE buffer supplemented with protease inhibitor and centrifuged for 1.5 h at 270,000 *g* at 4°C.

Chloroplast membrane washes

Normal and *dek5* chloroplasts were isolated and diluted to 1 mg chlorophyll per milliliter in import buffer. For each wash condition, 100 µl of chloroplasts was pelleted and resuspended in 0.1 M Na_2CO_3, pH 11.5, 6 M urea in 10 mM Hepes/KOH, pH 7.6, or 1 M NaCl. Each wash was held at room temperature for

30 min. Freeze–thaw lysis, as described for chloroplast fractionation, was used as a control. Treated chloroplasts were centrifuged at 40,000 *g* for 1 h at 4°C. Pellets were resuspended in TE on an equal volume basis with supernatants before SDS-PAGE and immunoblotting.

Protease protection assay

The dual protease protection assay was done according to Froehlich (2011) with some modifications. Intact chloroplasts were isolated and suspended in import buffer (0.33 M sorbitol and 50 mM Hepes/KOH, pH 8.0) to a concentration of 1 mg/ml chlorophyll. Intact chloroplasts (150 µl) were incubated with either 25 µl thermolysin or trypsin (1 mg/ml) for 50 min on ice. Thermolysin was stopped using 10 mM EDTA and kept on ice for 5 min. The trypsin digestion was stopped using 50 µl of protease inhibitors containing 1 mg/ml trypsin inhibitor (Sigma), 10 µM/ml leupeptin, and 10 mM PMSF. Intact chloroplasts were recovered using 30% Percoll cushion in import buffer and centrifuged at 1,500 *g* for 5 min. Pelleted intact chloroplasts were washed and resuspended in import buffer for further analysis.

Proteome analysis of the *dek5* chloroplast envelope and its normal siblings

To collect enough chloroplast envelope proteins for proteome analysis, six independent chloroplast preps from *dek5* and four independent chloroplast preps from normal siblings were pooled separately and resuspended to 1–2 mg/ml chlorophyll in suspension buffer (0.6 M sucrose, 10 mM tricine, and 2 mM EDTA, pH 7.5). Both the *dek5* and normal chloroplasts were lysed with two cycles of snap freezing and thawing and then diluted with TE buffer containing protease inhibitor cocktail to 0.2 M sucrose. A Dounce homogenizer was used to further rupture the *dek5* chloroplasts. Lysed chloroplasts were centrifuged at 4,000 *g* for 15 min to remove most of the thylakoid membranes. The supernatant was transferred to a new tube and centrifuged at 40,000 *g* for 60 min to collect crude envelope membrane fraction. Enriched chloroplast envelope proteins were solubilized in 8M urea, 100 mM Tris-HCl, pH 7, and 5 mM Tris-(2-carboxyethyl) phosphine, hydrochloride (TCEP). Proteins were then subjected to four rounds of acetone precipitation with probe sonication between each round. Pelleted protein was solubilized in UA buffer (8 M urea, 50 mM Tris-HCl, pH 7, and 5 mM TCEP) and processed using the filter-aided sample preparation method (Wiśniewski et al., 2009; Song et al., 2017) with microcon YM-30 centrifugal filters (Millipore). Proteins were digested on the filter overnight with 1 µg trypsin (Roche) at 37°C. Proteins were then further digested with 0.1 µg of trypsin and 0.1 µg of LysC (Wako) for 2 h. Recovered peptides were acidified to a pH of ∼2–3 with formic acid and desalted with 50 mg Sep-Pak C18 cartridges (Waters). Eluted peptides were dried in a vacuum centrifuge, resuspended in 0.1% formic acid, and quantified using the Pierce BCA Protein assay kit.

1 µg of peptides were separated on a 20-cm nanospray column, which was pulled and packed in-house with 2.5 µm C18 (Waters), using an acetonitrile gradient of 5–30% for 120 min, 30–80% for 25 min, and 0% for 5 min (150 min total) that was delivered via an Agilent 1260 quaternary HPLC at a flow rate of ∼500 nl/min. The HPLC system was coupled with a Thermo Scientific Q-Exactive Plus high-resolution quadrupole Orbitrap mass spectrometer using a custom-fabricated nanospray source. Data-dependent acquisition was obtained using Xcalibur 4.0 software in positive-ion mode with a spray voltage of 2.00 kV, radio frequency of 60, and a capillary temperature of 275°C. MS1 spectra were measured at a resolution of 70,000 with an automatic gain control of 3×10^6, a maximum ion time of 100 ms, and a mass range of 400–2,000 m/z. Up to 15 MS2, with a charge state of 2 to 4, were triggered at a resolution of 17,500, an automatic gain control of 10^5 with a maximum ion time of 50 ms, a 1.5-m/z isolation window, and a normalized collision energy of 28. MS1 that triggered MS2 scans were dynamically excluded for 25 s. We performed two runs for each sample to generate two technical replicates.

The raw data were searched against the B73 RefGen_v2 5b Filtered Gene Set using MaxQuant version 1.5.8.3 (Tyanova et al., 2016). Methionine oxidation and protein N-terminal acetylation were set as variable modifications. The digestion parameters were set to "specific" for "Trypsin/P;LysC" with a maximum of two missed cleavages. The match between runs feature was turned off. Default settings were used for the remaining parameters including a peptide spectrum match and protein false discovery rate of 0.01, which was determined using a reverse decoy database.

The *dek5* mutant and normal sibling envelope protein extracts had different levels of nonenvelope contaminants. To compare relative levels of envelope proteins, we curated a set of 96 envelope proteins that were validated experimentally. The MaxQuant intensity for the 85 envelope peptides within this subset found in at least one technical replicate were normalized relative to one normal technical replicate. Proteins identified in a single technical replicate with a normalized MaxQuant intensity value $<10^7$ were removed to leave 68 proteins. Relative fold change between *dek5* and normal sibling samples were calculated from the average of the two technical replicates or the single MaxQuant intensity value if the protein was detected only once. TMDs for envelope proteins were predicted using TMHMM Server V2.0 (http://www.cbs.dtu.dk/services/TMHMM/), and envelope localization was annotated using the Plant Proteome Database (Sun et al., 2009).

$^{32}P_i$ chloroplast uptake assay

Uptake of $^{32}P_i$ into isolated chloroplasts was assayed as described with some modifications (Fliege et al., 1978). Purified, intact chloroplasts from B73 and *dek5-N961* mutants were adjusted in concentration to OD_{652} of 0.2 and 90 µl (∼2.3×10^7 normal and 4.6×10^6 *dek5*) chloroplasts were mixed with 10 µl 1 mM KH_2PO_4, pH 7.5. KH_2PO_4 was prepared in a 19:1 ratio of unlabeled to radiolabeled 37 MBq/mM $KH_2{}^{32}PO_4$ (PerkinElmer). Chloroplasts were incubated in a time course from 5 to 300 s. Phosphate uptake was stopped by adding 2 mM 4,4′-diisothiocyanatostilbene-2,2′-disulfonic acid (DIDS; Sigma) to the reaction. Relative uptake was calculated from background radiolabel as determined by preincubating chloroplasts with DIDS for 5 min before incubating with $^{32}P_i$ for 300 s. Intact normal chloroplasts with radiolabel were repurified by transferring 100 µl of the

chloroplast suspension to a centrifuge tube containing a lower layer of 30 µl of 10% perchloric acid and an upper layer of 70 µl AP 150 silicone oil (Wacker). The density of *dek5* mutant chloroplasts was lower than normal, and intact chloroplasts were purified using a 4:1 mixture of AP 150 and AR 20 silicone oil (Sigma). The radiolabeled chloroplast suspension was overlaid onto the silicone oil and then centrifuged for 30 s at 14,000 *g*. The radiolabel associated with intact chloroplasts was assayed by sampling 15 µl of the 10% perchloric acid layer for scintillation counting using a Beckman LS6500SE scintillation counter.

Detection limits were determined after a 300-s incubation with normal chloroplasts diluted from 5% to 50% of an OD_{652} of 0.2. Mutant chloroplasts were concentrated by centrifugation of two- and fourfold larger volumes at 500 *g* for 1 min followed by resuspension in 90 µl of 0.7 M sorbitol and 50 mM Hepes-KOH, pH 7.5. Stromal volume was estimated by counting intact chloroplasts and multiplying by the average stromal volume estimated from TEM. Chloroplasts were counted in a hemocytometer using a Zeiss Standard WL microscope with a Neofluor 40×/0.75 objective at room temperature.

Assay effects on chloroplast integrity was determined by incubating chloroplasts with 0.1 mM KH_2PO_4, pH 7.5, for 300 s. Chloroplasts were repurified through silicone oil with a bottom layer of 30 µl of 50 mM Hepes-KOH, pH 7.5, and 0.3 M or 0.7 M sorbitol for normal and *dek5* mutants, respectively. Pelleted, intact chloroplasts were washed twice with the sorbitol buffer to remove residual silicone oil, observed at room temperature under a Zeiss Standard WL microscope with a Neofluor 40×/0.75 objective with a phase-contrast condenser. Microscopy images were captured with an AMScope MU500 digital camera with AMscope acquisition software version 3.7 for a Windows 64-bit operating system.

Online supplemental material

Fig. S1 shows the influence of different genetic backgrounds on *dek5* kernel and plant phenotypes. Fig. S2 provides additional TEM images showing the range of chloroplast defects in *dek5*. Fig. S3 is a multiple sequence alignment of N-terminal DEK5 protein sequences showing conserved regions used to determine sites for GFP fusion protein constructs. Fig. S4 shows control experiments for the DEK5 antibody and biological replicates of experiments in Fig. 9. Table S1 lists data from the proteomic analysis of chloroplast envelope proteins. Table S2 lists the primers used in this study. Video 1 shows Z-stack images of chlorophyll autofluorescence in normal and *dek5* protoplasts to provide evidence for a lack of chlorophyll in the interior of some *dek5* chloroplasts.

Acknowledgments

We thank Richard Medville at the Electron Microscopy Services (Colorado Springs, CO) for TEM analysis. We thank the following collaborators for providing antibodies: Dr. Alice Barkan at the University of Oregon (Eugene, OR; OEC23, Cyt F, and CF1-β), Dr. Carole Dabney-Smith at Miami University (Miami, FL; Toc75), Dr. Antje von Schaewen at the University of Münster (Münster, Germany; 6PGDH), and Dr. Kentaro Inoue at University of California, Davis (Davis, CA; OEP80). We also thank Drs. L. Curtis Hannah and Ken Cline at the University of Florida for intellectual input.

This work was supported by the National Institute of Food and Agriculture (awards 2011-67003-30215 and 2018-51181-28419), the China Scholarship Council, and the Vasil-Monsanto Endowment.

The authors declare no competing financial interests.

Author contributions: J. Zhang and A.M. Settles designed the research, performed experiments, analyzed data, and wrote the manuscript; S. Wu completed Mu-Seq, and D.R. McCarty analyzed the data; S.K. Boehlein measured ADP-glucose; G. Song and J. Walley performed the chloroplast envelope proteomics. A. Myers measured amylopectin chain distribution.

Submitted: 23 July 2018
Revised: 7 May 2019
Accepted: 4 June 2019

References

Azari, F., L. Nyland, C. Yu, M. Radermacher, K.P. Mintz, and T. Ruiz. 2013. Ultrastructural analysis of the rugose cell envelope of a member of the Pasteurellaceae family. *J. Bacteriol.* 195:1680–1688. https://doi.org/10.1128/JB.02149-12

Babu, M., C. Bundalovic-Torma, C. Calmettes, S. Phanse, Q. Zhang, Y. Jiang, Z. Minic, S. Kim, J. Mehla, A. Gagarinova, et al. 2018. Global landscape of cell envelope protein complexes in Escherichia coli. *Nat. Biotechnol.* 36: 103–112. https://doi.org/10.1038/nbt.4024

Baldwin, A., A. Wardle, R. Patel, P. Dudley, S.K. Park, D. Twell, K. Inoue, and P. Jarvis. 2005. A molecular-genetic study of the Arabidopsis Toc75 gene family. *Plant Physiol.* 138:715–733. https://doi.org/10.1104/pp.105.063289

Barkan, A., D. Miles, and W.C. Taylor. 1986. Chloroplast gene expression in nuclear, photosynthetic mutants of maize. *EMBO J.* 5:1421–1427. https://doi.org/10.1002/j.1460-2075.1986.tb04378.x

Block, M.A., R. Douce, J. Joyard, and N. Rolland. 2007. Chloroplast envelope membranes: a dynamic interface between plastids and the cytosol. *Photosynth. Res.* 92:225–244. https://doi.org/10.1007/s11120-007-9195-8

Bölter, B., and J. Soll. 2016. Once upon a time-chloroplast protein import research from infancy to future challenges. *Mol. Plant.* 9:798–812. https://doi.org/10.1016/j.molp.2016.04.014

Bowsher, C.G., and A.K. Tobin. 2001. Compartmentation of metabolism within mitochondria and plastids. *J. Exp. Bot.* 52:513–527. https://doi.org/10.1093/jexbot/52.356.513

Breuers, F.K., A. Bräutigam, S. Geimer, U.Y. Welzel, G. Stefano, L. Renna, F. Brandizzi, and A.P. Weber. 2012. Dynamic Remodeling of the Plastid Envelope Membranes - A Tool for Chloroplast Envelope in vivo Localizations. *Front. Plant Sci.* 3:7. https://doi.org/10.3389/fpls.2012.00007

Chen, Y.-L., L.-J. Chen, C.-C. Chu, P.-K. Huang, J.-R. Wen, and H.M. Li. 2018. TIC236 links the outer and inner membrane translocons of the chloroplast. *Nature.* 564:125–129. https://doi.org/10.1038/s41586-018-0713-y

Cline, K., and C. Dabney-Smith. 2008. Plastid protein import and sorting: different paths to the same compartments. *Curr. Opin. Plant Biol.* 11: 585–592. https://doi.org/10.1016/j.pbi.2008.10.008

Facchinelli, F., and A.P.M. Weber. 2011. The metabolite transporters of the plastid envelope: an update. *Front. Plant Sci.* 2:50. https://doi.org/10.3389/fpls.2011.00050

Fischer, K. 2011. The import and export business in plastids: transport processes across the inner envelope membrane. *Plant Physiol.* 155:1511–1519. https://doi.org/10.1104/pp.110.170241

Fliege, R., U.-I. Flügge, K. Werdan, and H.W. Heldt. 1978. Specific transport of inorganic phosphate, 3-phosphoglycerate and triosephosphates across the inner membrane of the envelope in spinach chloroplasts. *Biochim. Biophys. Acta.* 502:232–247. https://doi.org/10.1016/0005-2728(78)90045-2

Flügge, U.-I. 1999. Phosphate translocators in plastids. *Annu. Rev. Plant Physiol. Plant Mol. Biol.* 50:27–45. https://doi.org/10.1146/annurev.arplant.50.1.27

Flügge, U.I., and R. Benz. 1984. Pore-forming activity in the outer membrane of the chloroplast envelope. *FEBS Lett.* 169:85–89. https://doi.org/10.1016/0014-5793(84)80294-X

Fristedt, R., R. Williams-Carrier, S.S. Merchant, and A. Barkan. 2014. A thylakoid membrane protein harboring a DnaJ-type zinc finger domain is required for photosystem I accumulation in plants. *J. Biol. Chem.* 289: 30657–30667. https://doi.org/10.1074/jbc.M114.587758

Froehlich, J. 2011. Studying Arabidopsis envelope protein localization and topology using thermolysin and trypsin proteases. *In Chloroplast Research in Arabidopsis: Methods and Protocols.* Vol. I. R.P. Jarvis, editor. Humana Press 351–367. https://doi.org/10.1007/978-1-61779-234-2_21

Gallant, C.V., M. Sedic, E.A. Chicoine, T. Ruiz, and K.P. Mintz. 2008. Membrane morphology and leukotoxin secretion are associated with a novel membrane protein of Aggregatibacter actinomycetemcomitans. *J. Bacteriol.* 190:5972–5980. https://doi.org/10.1128/JB.00548-08

Gibon, Y., H. Vigeolas, A. Tiessen, P. Geigenberger, and M. Stitt. 2002. Sensitive and high throughput metabolite assays for inorganic pyrophosphate, ADPGlc, nucleotide phosphates, and glycolytic intermediates based on a novel enzymic cycling system. *Plant J.* 30:221–235. https://doi.org/10.1046/j.1365-313X.2001.01278.x

Goetze, T.A., K. Philippar, I. Ilkavets, J. Soll, and R. Wagner. 2006. OEP37 is a new member of the chloroplast outer membrane ion channels. *J. Biol. Chem.* 281:17989–17998. https://doi.org/10.1074/jbc.M600700200

Gould, S.B., R.F. Waller, and G.I. McFadden. 2008. Plastid evolution. *Annu. Rev. Plant Biol.* 59:491–517. https://doi.org/10.1146/annurev.arplant.59.032607.092915

Gross, J., and D. Bhattacharya. 2009. Mitochondrial and plastid evolution in eukaryotes: an outsiders' perspective. *Nat. Rev. Genet.* 10:495–505. https://doi.org/10.1038/nrg2610

Hagan, C.L., T.J. Silhavy, and D. Kahne. 2011. β-Barrel membrane protein assembly by the Bam complex. *Annu. Rev. Biochem.* 80:189–210. https://doi.org/10.1146/annurev-biochem-061408-144611

Hannah, L.C. 1997. Starch synthesis in the maize seed. *In Cellular and Molecular Biology of Plant Seed Development.* B.A. Larkins and I.K. Vasil, editors. Springer, Netherlands. 375–405. https://doi.org/10.1007/978-94-015-8909-3_10

Harsman, A., A. Schock, B. Hemmis, V. Wahl, I. Jeshen, P. Bartsch, A. Schlereth, H. Pertl-Obermeyer, T.A. Goetze, J. Soll, et al. 2016. OEP40, a Regulated Glucose-permeable β-Barrel Solute Channel in the Chloroplast Outer Envelope Membrane. *J. Biol. Chem.* 291:17848–17860. https://doi.org/10.1074/jbc.M115.712398

Hedges, S.B. 1992. The number of replications needed for accurate estimation of the bootstrap P value in phylogenetic studies. *Mol. Biol. Evol.* 9: 366–369.

Heinz, E., J. Selkrig, M.J. Belousoff, and T. Lithgow. 2015. Evolution of the translocation and assembly module (TAM). *Genome Biol. Evol.* 7: 1628–1643. https://doi.org/10.1093/gbe/evv097

Hemmler, R., T. Becker, E. Schleiff, B. Bölter, T. Stahl, J. Soll, T.A. Götze, S. Braams, and R. Wagner. 2006. Molecular properties of Oep21, an ATP-regulated anion-selective solute channel from the outer chloroplast membrane. *J. Biol. Chem.* 281:12020–12029. https://doi.org/10.1074/jbc.M513586200

Hoiczyk, E., and A. Hansel. 2000. Cyanobacterial cell walls: news from an unusual prokaryotic envelope. *J. Bacteriol.* 182:1191–1199. https://doi.org/10.1128/JB.182.5.1191-1199.2000

Hölscher, C., M.-C. Lutterbey, H. Lansing, T. Meyer, K. Fischer, and A. von Schaewen. 2016. Defects in peroxisomal 6-phosphogluconate dehydrogenase isoform PGD2 prevent gametophytic interaction in Arabidopsis thaliana. *Plant Physiol.* 171:192–205. https://doi.org/10.1104/pp.15.01301

Huang, B., T.A. Hennen-Bierwagen, and A.M. Myers. 2014. Functions of multiple genes encoding ADP-glucose pyrophosphorylase subunits in maize endosperm, embryo, and leaf. *Plant Physiol.* 164:596–611. https://doi.org/10.1104/pp.113.231605

Huang, W., Q. Ling, J. Bédard, K. Lilley, and P. Jarvis. 2011. In vivo analyses of the roles of essential Omp85-related proteins in the chloroplast outer envelope membrane. *Plant Physiol.* 157:147–159. https://doi.org/10.1104/pp.111.181891

Hust, B., and M. Gutensohn. 2006. Deletion of core components of the plastid protein import machinery causes differential arrest of embryo development in Arabidopsis thaliana. *Plant Biol (Stuttg).* 8:18–30. https://doi.org/10.1055/s-2005-873044

Ii, J.A., and A.N. Webber. 2005. Photosynthesis in Arabidopsis thaliana mutants with reduced chloroplast number. *Photosynth. Res.* 85:373–384. https://doi.org/10.1007/s11120-005-7708-x

Inoue, K., and D. Potter. 2004. The chloroplastic protein translocation channel Toc75 and its paralog OEP80 represent two distinct protein families and are targeted to the chloroplastic outer envelope by different mechanisms. *Plant J.* 39:354–365. https://doi.org/10.1111/j.1365-313X.2004.02135.x

Iqbal, H., M.R. Kenedy, M. Lybecker, and D.R. Akins. 2016. The TamB ortholog of Borrelia burgdorferi interacts with the β-barrel assembly machine (BAM) complex protein BamA. *Mol. Microbiol.* 102:757–774. https://doi.org/10.1111/mmi.13492

Itoh, R., M. Fujiwara, N. Nagata, and S. Yoshida. 2001. A chloroplast protein homologous to the eubacterial topological specificity factor minE plays a role in chloroplast division. *Plant Physiol.* 127:1644–1655. https://doi.org/10.1104/pp.010386

Jarvis, P. 2008. Targeting of nucleus-encoded proteins to chloroplasts in plants. *New Phytol.* 179:257–285. https://doi.org/10.1111/j.1469-8137.2008.02452.x

Jarvis, P., and E. López-Juez. 2013. Biogenesis and homeostasis of chloroplasts and other plastids. *Nat. Rev. Mol. Cell Biol.* 14:787–802. https://doi.org/10.1038/nrm3702

Kamau, P.K., S. Sano, T. Takami, R. Matsushima, M. Maekawa, and W. Sakamoto. 2015. A mutation in GIANT CHLOROPLAST encoding a PARC6 homolog affects spikelet fertility in rice. *Plant Cell Physiol.* 56:977–991. https://doi.org/10.1093/pcp/pcv024

Karamoko, M., S. El-Kafafi, P. Mandaron, S. Lerbs-Mache, and D. Falconet. 2011. Multiple FtsZ2 isoforms involved in chloroplast division and biogenesis are developmentally associated with thylakoid membranes in Arabidopsis. *FEBS Lett.* 585:1203–1208. https://doi.org/10.1016/j.febslet.2011.03.041

Karimi, M., D. Inzé, and A. Depicker. 2002. GATEWAY vectors for Agrobacterium-mediated plant transformation. *Trends Plant Sci.* 7: 193–195. https://doi.org/10.1016/S1360-1385(02)02251-3

Karimi, M., A. Depicker, and P. Hilson. 2007. Recombinational cloning with plant gateway vectors. *Plant Physiol.* 145:1144–1154. https://doi.org/10.1104/pp.107.106989

Kasmati, A.R., M. Töpel, R. Patel, G. Murtaza, and P. Jarvis. 2011. Molecular and genetic analyses of Tic20 homologues in Arabidopsis thaliana chloroplasts. *Plant J.* 66:877–889. https://doi.org/10.1111/j.1365-313X.2011.04551.x

Keegstra, K., and K. Cline. 1999. Protein import and routing systems of chloroplasts. *Plant Cell.* 11:557–570. https://doi.org/10.1105/tpc.11.4.557

Kovacheva, S., J. Bédard, R. Patel, P. Dudley, D. Twell, G. Ríos, C. Koncz, and P. Jarvis. 2005. In vivo studies on the roles of Tic110, Tic40 and Hsp93 during chloroplast protein import. *Plant J.* 41:412–428. https://doi.org/10.1111/j.1365-313X.2004.02307.x

Larkin, M.A., G. Blackshields, N.P. Brown, R. Chenna, P.A. McGettigan, H. McWilliam, F. Valentin, I.M. Wallace, A. Wilm, R. Lopez, et al. 2007. Clustal W and Clustal X version 2.0. *Bioinformatics.* 23:2947–2948. https://doi.org/10.1093/bioinformatics/btm404

Lee, L., and C.Y. Tsai. 1984. Zein synthesis in the embryo and endosperm of maize mutants. *Biochem. Genet.* 22:729–737. https://doi.org/10.1007/BF00485856

Leegood, R.C. 2008. Roles of the bundle sheath cells in leaves of C3 plants. *J. Exp. Bot.* 59:1663–1673. https://doi.org/10.1093/jxb/erm335

Li, M., and D.J. Schnell. 2006. Reconstitution of protein targeting to the inner envelope membrane of chloroplasts. *J. Cell Biol.* 175:249–259. https://doi.org/10.1083/jcb.200605162

Lichtenthaler, H.K., and A.R. Wellburn. 1983. Determinations of total carotenoids and chlorophylls a and b of leaf extracts in different solvents. *Biochem. Soc. Trans.* 11:591–592. https://doi.org/10.1042/bst0110591

Lin, Q., B. Huang, M. Zhang, X. Zhang, J. Rivenbark, R.L. Lappe, M.G. James, A.M. Myers, and T.A. Hennen-Bierwagen. 2012. Functional interactions between starch synthase III and isoamylase-type starch-debranching enzyme in maize endosperm. *Plant Physiol.* 158:679–692. https://doi.org/10.1104/pp.111.189704

Ma, Y., A. Kouranov, S.E. LaSala, and D.J. Schnell. 1996. Two components of the chloroplast protein import apparatus, IAP86 and IAP75, interact with the transit sequence during the recognition and translocation of precursor proteins at the outer envelope. *J. Cell Biol.* 134:315–327. https://doi.org/10.1083/jcb.134.2.315

Machettira, A.B., L.E. Groß, B. Tillmann, B.L. Weis, G. Englich, M.S. Sommer, M. Königer, and E. Schleiff. 2012. Protein-induced modulation of chloroplast membrane morphology. *Front. Plant Sci.* 2:118. https://doi.org/10.3389/fpls.2011.00118

Majeran, W., Y. Cai, Q. Sun, and K.J. van Wijk. 2005. Functional differentiation of bundle sheath and mesophyll maize chloroplasts determined by comparative proteomics. *Plant Cell.* 17:3111–3140. https://doi.org/10.1105/tpc.105.035519

Maple, J., L. Vojta, J. Soll, and S.G. Møller. 2007. ARC3 is a stromal Z-ring accessory protein essential for plastid division. *EMBO Rep.* 8:293–299. https://doi.org/10.1038/sj.embor.7400902

Matsushima, R., M. Maekawa, M. Kusano, H. Kondo, N. Fujita, Y. Kawagoe, and W. Sakamoto. 2014. Amyloplast-localized SUBSTANDARD STARCH GRAIN4 protein influences the size of starch grains in rice endosperm. *Plant Physiol.* 164:623–636. https://doi.org/10.1104/pp.113.229591

McCarty, D.R., S. Latshaw, S. Wu, M. Suzuki, C.T. Hunter, W.T. Avigne, and K.E. Koch. 2013. Mu-seq: sequence-based mapping and identification of transposon induced mutations. *PLoS One.* 8:e77172. https://doi.org/10.1371/journal.pone.0077172

Neuffer, M.G., and W.F. Sheridan. 1980. Defective kernel mutants of maize. I. Genetic and lethality studies. *Genetics.* 95:929–944.

Nikaido, H. 1994. Porins and specific diffusion channels in bacterial outer membranes. *J. Biol. Chem.* 269:3905–3908.

Oikawa, K., A. Yamasato, S.-G. Kong, M. Kasahara, M. Nakai, F. Takahashi, Y. Ogura, T. Kagawa, and M. Wada. 2008. Chloroplast outer envelope protein CHUP1 is essential for chloroplast anchorage to the plasma membrane and chloroplast movement. *Plant Physiol.* 148:829–842. https://doi.org/10.1104/pp.108.123075

Okawa, K., K. Nakayama, T. Kakizaki, T. Yamashita, and T. Inaba. 2008. Identification and characterization of Cor413im proteins as novel components of the chloroplast inner envelope. *Plant Cell Environ.* 31:1470–1483. https://doi.org/10.1111/j.1365-3040.2008.01854.x

Pogson, B.J., D. Ganguly, and V. Albrecht-Borth. 2015. Insights into chloroplast biogenesis and development. *Biochim. Biophys. Acta.* 1847:1017–1024. https://doi.org/10.1016/j.bbabio.2015.02.003

Pohlmeyer, K., J. Soll, T. Steinkamp, S. Hinnah, and R. Wagner. 1997. Isolation and characterization of an amino acid-selective channel protein present in the chloroplastic outer envelope membrane. *Proc. Natl. Acad. Sci. USA.* 94:9504–9509. https://doi.org/10.1073/pnas.94.17.9504

Pohlmeyer, K., J. Soll, R. Grimm, K. Hill, and R. Wagner. 1998. A high-conductance solute channel in the chloroplastic outer envelope from Pea. *Plant Cell.* 10:1207–1216. https://doi.org/10.1105/tpc.10.7.1207

Pudelski, B., A. Schock, S. Hoth, R. Radchuk, H. Weber, J. Hofmann, U. Sonnewald, J. Soll, and K. Philippar. 2012. The plastid outer envelope protein OEP16 affects metabolic fluxes during ABA-controlled seed development and germination. *J. Exp. Bot.* 63:1919–1936. https://doi.org/10.1093/jxb/err375

Pyke, K.A., and R.M. Leech. 1992. Chloroplast Division and Expansion Is Radically Altered by Nuclear Mutations in Arabidopsis thaliana. *Plant Physiol.* 99:1005–1008. https://doi.org/10.1104/pp.99.3.1005

Pyke, K.A., S.M. Rutherford, E.J. Robertson, and R.M. Leech. 1994. arc6, a fertile Arabidopsis mutant with only two mesophyll cell chloroplasts. *Plant Physiol.* 106:1169–1177. https://doi.org/10.1104/pp.106.3.1169

Robertson, E.J., S.M. Rutherford, and R.M. Leech. 1996. Characterization of chloroplast division using the Arabidopsis mutant arc5. *Plant Physiol.* 112:149–159. https://doi.org/10.1104/pp.112.1.149

Sachs, M.M. 2009. Maize genetic resources. *In Molecular Genetic Approaches to Maize Improvement.* A.L.K.A. Larkins, editor. Springer, Berlin, Heidelberg. 197–209. https://doi.org/10.1007/978-3-540-68922-5_14

Scanlon, M.J., P.S. Stinard, M.G. James, A.M. Myers, and D.S. Robertson. 1994. Genetic analysis of 63 mutations affecting maize kernel development isolated from Mutator stocks. *Genetics.* 136:281–294.

Schindelin, J., I. Arganda-Carreras, E. Frise, V. Kaynig, M. Longair, T. Pietzsch, S. Preibisch, C. Rueden, S. Saalfeld, B. Schmid, et al. 2012. Fiji: an open-source platform for biological-image analysis. *Nat. Methods.* 9:676–682. https://doi.org/10.1038/nmeth.2019

Schleiff, E., J. Soll, M. Küchler, W. Kühlbrandt, and R. Harrer. 2003. Characterization of the translocon of the outer envelope of chloroplasts. *J. Cell Biol.* 160:541–551. https://doi.org/10.1083/jcb.200210060

Selkrig, J., K. Mosbahi, C.T. Webb, M.J. Belousoff, A.J. Perry, T.J. Wells, F. Morris, D.L. Leyton, M. Totsika, M.-D. Phan, et al. 2012. Discovery of an archetypal protein transport system in bacterial outer membranes. *Nat. Struct. Mol. Biol.* 19:506–510: S1. https://doi.org/10.1038/nsmb.2261

Selkrig, J., D.L. Leyton, C.T. Webb, and T. Lithgow. 2014. Assembly of β-barrel proteins into bacterial outer membranes. *Biochim. Biophys. Acta.* 1843:1542–1550. https://doi.org/10.1016/j.bbamcr.2013.10.009

Settles, A.M., A.M. Bagadion, F. Bai, J. Zhang, B. Barron, K. Leach, J.S. Mudunkothge, C. Hoffner, S. Bihmidine, E. Finefield, et al. 2014. Efficient molecular marker design using the MaizeGDB Mo17 SNPs and Indels track. *G3 (Bethesda).* 4:1143–1145. https://doi.org/10.1534/g3.114.010454

Shannon, J.C., F.M. Pien, and K.C. Liu. 1996. Nucleotides and Nucleotide Sugars in Developing Maize Endosperms (Synthesis of ADP-Glucose in brittle-1). *Plant Physiol.* 110:835–843. https://doi.org/10.1104/pp.110.3.835

Shannon, J.C., F.-M. Pien, H. Cao, and K.-C. Liu. 1998. Brittle-1, an adenylate translocator, facilitates transfer of extraplastidial synthesized ADP--glucose into amyloplasts of maize endosperms. *Plant Physiol.* 117:1235–1252. https://doi.org/10.1104/pp.117.4.1235

Shen, H.-H., D.L. Leyton, T. Shiota, M.J. Belousoff, N. Noinaj, J. Lu, S.A. Holt, K. Tan, J. Selkrig, C.T. Webb, et al. 2014. Reconstitution of a nanomachine driving the assembly of proteins into bacterial outer membranes. *Nat. Commun.* 5:5078–5078. https://doi.org/10.1038/ncomms6078

Shimada, H., M. Koizumi, K. Kuroki, M. Mochizuki, H. Fujimoto, H. Ohta, T. Masuda, and K. Takamiya. 2004. ARC3, a chloroplast division factor, is a chimera of prokaryotic FtsZ and part of eukaryotic phosphatidylinositol-4-phosphate 5-kinase. *Plant Cell Physiol.* 45:960–967. https://doi.org/10.1093/pcp/pch130

Singh, N.D., M. Li, S.-B. Lee, D. Schnell, and H. Daniell. 2008. Arabidopsis Tic40 expression in tobacco chloroplasts results in massive proliferation of the inner envelope membrane and upregulation of associated proteins. *Plant Cell.* 20:3405–3417. https://doi.org/10.1105/tpc.108.063172

Smith, M.D., D.J. Schnell, L. Fitzpatrick, and K. Keegstra. 2003. In vitro analysis of chloroplast protein import. *Curr. Protoc. Cell Biol.* Chapter 11: Unit 11.16.

Song, G., M.R. McReynolds, and J.W. Walley. 2017. Sample preparation protocols for protein abundance, acetylome, and phosphoproteome profiling of plant tissues. *Methods Mol. Biol.* 1610:123–133. https://doi.org/10.1007/978-1-4939-7003-2_9

Sun, Q., B. Zybailov, W. Majeran, G. Friso, P.D. Olinares, and K.J. van Wijk. 2009. PPDB, the Plant Proteomics Database at Cornell. *Nucleic Acids Res.* 37(suppl_1):D969–D974. https://doi.org/10.1093/nar/gkn654

Szczepanik, J., and P. Sowiński. 2014. The occurrence of chloroplast peripheral reticulum in grasses: a matter of phylogeny or a matter of function? *Acta Physiol. Plant.* 36:1133–1142. https://doi.org/10.1007/s11738-014-1488-x

Theg, S.M., C. Bauerle, L.J. Olsen, B.R. Selman, and K. Keegstra. 1989. Internal ATP is the only energy requirement for the translocation of precursor proteins across chloroplastic membranes. *J. Biol. Chem.* 264:6730–6736.

Tobias, R.B., C.D. Boyer, and J.C. Shannon. 1992. Alterations in Carbohydrate Intermediates in the Endosperm of Starch-Deficient Maize (Zea mays L.) Genotypes. *Plant Physiol.* 99:146–152. https://doi.org/10.1104/pp.99.1.146

Tripp, J., K. Inoue, K. Keegstra, and J.E. Froehlich. 2007. A novel serine/proline-rich domain in combination with a transmembrane domain is required for the insertion of AtTic40 into the inner envelope membrane of chloroplasts. *Plant J.* 52:824–838. https://doi.org/10.1111/j.1365-313X.2007.03279.x

Turgeon, R., and R. Medville. 2004. Phloem loading. A reevaluation of the relationship between plasmodesmatal frequencies and loading strategies. *Plant Physiol.* 136:3795–3803. https://doi.org/10.1104/pp.104.042036

Tyanova, S., T. Temu, and J. Cox. 2016. The MaxQuant computational platform for mass spectrometry-based shotgun proteomics. *Nat. Protoc.* 11:2301–2319. https://doi.org/10.1038/nprot.2016.136

Tzafrir, I., R. Pena-Muralla, A. Dickerman, M. Berg, R. Rogers, S. Hutchens, T.C. Sweeney, J. McElver, G. Aux, D. Patton, and D. Meinke. 2004. Identification of genes required for embryo development in Arabidopsis. *Plant Physiol.* 135:1206–1220. https://doi.org/10.1104/pp.104.045179

van Doorn, W.G., E.P. Beers, J.L. Dangl, V.E. Franklin-Tong, P. Gallois, I. Hara-Nishimura, A.M. Jones, M. Kawai-Yamada, E. Lam, J. Mundy, et al. 2011. Morphological classification of plant cell deaths. *Cell Death Differ.* 18:1241–1246. https://doi.org/10.1038/cdd.2011.36

van Esse, H.P. 2012. Identification of HR-inducing cDNAs from plant pathogens via a Gateway®-compatible binary potato virus X-expression vector. *In Plant Fungal Pathogens.* M.D. Bolton and B.P.H.J. Thomma, editors. Springer. 97–105. https://doi.org/10.1007/978-1-61779-501-5_6

Viana, A.A.B., M. Li, and D.J. Schnell. 2010. Determinants for stop-transfer and post-import pathways for protein targeting to the chloroplast inner envelope membrane. *J. Biol. Chem.* 285:12948–12960. https://doi.org/10.1074/jbc.M110.109744

Voelker, R., and A. Barkan. 1995. Two nuclear mutations disrupt distinct pathways for targeting proteins to the chloroplast thylakoid. *EMBO J.* 14:3905–3914. https://doi.org/10.1002/j.1460-2075.1995.tb00062.x

Weigel, D., and J. Glazebrook. 2006. Transformation of Agrobacterium Using the Freeze-Thaw Method. *CSH Protoc*. 2006.

Weise, S.E., K.J. van Wijk, and T.D. Sharkey. 2011. The role of transitory starch in C(3), CAM, and C(4) metabolism and opportunities for engineering leaf starch accumulation. *J. Exp. Bot.* 62:3109–3118. https://doi.org/10.1093/jxb/err035

Wise, R.R. 2007. The diversity of plastid form and function. *In The Structure and Function of Plastids*. R.R.W.K. Hoober, editor. Springer, Dordrecht. 3–26. https://doi.org/10.1007/978-1-4020-4061-0_1

Wiśniewski, J.R., A. Zougman, N. Nagaraj, and M. Mann. 2009. Universal sample preparation method for proteome analysis. *Nat. Methods.* 6: 359–362. https://doi.org/10.1038/nmeth.1322

Wu, Y., and J. Messing. 2012. RNA interference can rebalance the nitrogen sink of maize seeds without losing hard endosperm. *PLoS One.* 7:e32850. https://doi.org/10.1371/journal.pone.0032850

Yoo, S.-D., Y.-H. Cho, and J. Sheen. 2007. Arabidopsis mesophyll protoplasts: a versatile cell system for transient gene expression analysis. *Nat. Protoc.* 2:1565–1572. https://doi.org/10.1038/nprot.2007.199

Yoon, H.S., J.D. Hackett, C. Ciniglia, G. Pinto, and D. Bhattacharya. 2004. A molecular timeline for the origin of photosynthetic eukaryotes. *Mol. Biol. Evol.* 21:809–818. https://doi.org/10.1093/molbev/msh075

Yu, J., T. Li, S. Dai, Y. Weng, J. Li, Q. Li, H. Xu, Y. Hua, and B. Tian. 2017. A tamB homolog is involved in maintenance of cell envelope integrity and stress resistance of Deinococcus radiodurans. *Sci. Rep.* 7:45929. https://doi.org/10.1038/srep45929